m6A regulates ADAR1-mediated RNA editing during macrophage activation

Valerie Griesche[1,2†], Salvatore Di Giorgio[1†*], Julia Brettschneider[5], Chih-Yuan Kao[2,3], Irem Tellioglu[2,4], Laura Pezzella[1,2], Jose Paulo Lorenzo[1], Annette Arnold[1], Riccardo Pecori[1], Georg Stoecklin[3], F. Nina Papavasiliou[1*]

1 Division of Immune Diversity, German Cancer Research Center, Heidelberg 69120, Germany.
2 Graduate Program of Faculty of Biosciences, Heidelberg University, Heidelberg 69120, Germany.
3 Mannheim Institute for Innate Immunoscience (MI3) and Mannheim Cancer Center (MCC), Medical Faculty Mannheim, Heidelberg University, Mannheim 68167, Germany; and Center for Molecular Biology of Heidelberg University (ZMBH), German Cancer Research Center (DKFZ)-ZMBH Alliance, Heidelberg, Germany
4 Division of Cancer Epigenomics, German Cancer Research Center, Heidelberg 69120, Germany.
5 Department of Statistics, University of Warwick, Coventry, CV4 7AL, UK.

† These authors contributed equally to this work.
*Correspondence: salvatore.digiorgio@dkfz.de, n.papavasiliou@dkfz.de

Abstract

Macrophages are a highly plastic innate immune cell subset that depends on environmental cues to activate, execute and resolve inflammatory responses. This plasticity of function is mirrored by the diversity of RNA modifications that dynamically decorate macrophage transcripts. Here, using the mouse macrophage line RAW 264.7 (RAW), we addressed the combinatorial effect of two major mRNA modifications: adenosine to inosine (A-to-I) deamination by ADAR1 and adenosine N6-methylation (m6A) by METTL3. Using both short-read and single molecule sequencing on RAW macrophages with genetic deletions of ADAR1 or METTL3, we identified transcripts that were modified by both enzymes, with specific functional outcomes on macrophage activation. While m6A levels remained relatively stable even in the absence of ADAR1, loss of METTL3 led to a global reduction in A-to-I editing levels. This interrelation was most apparent when m6A sites were distant from sites of deamination, suggesting a possible function of m6A in ADAR1-mediated editing. Using a dual reporter cell line where guided ADAR1 recruitment can be measured via eGFP reactivation, we observed that m6A modification of ADAR-engager guide RNAs substantially improved targeted RNA editing. Overall, we report the first example of an interdependence between modifications, which can also be therapeutically exploited.

Introduction

Dynamic mRNA modifications have a crucial impact on the fate and metabolism of a transcript, including splicing, subcellular localization, stability, and translation[1]. N6-methyladenosine (m6A) and adenosine to inosine (A-to-I) editing are among the most prominent modifications found in mRNA[1]. The reversible methylation of adenosine (A) is catalyzed by the catalytic subunits Methyltransferase 3 (METTL3), which forms part of the core m6A writer complex together with Methyltransferase 14 (METTL14) and Wilms' tumor 1-associating protein (WTAP). The m6A writer complex preferably modifies A within the consensus DRACH (D = G/A/U, R = G/A, H = A/U/C)) motif[2–4]. Within the transcript, m6A sites are enriched after the last splice site of the last exon and in the 3' untranslated region (3'UTR) in proximity to the stop codon[1,2,5]. M6A can be removed from a transcript by eraser proteins fat mass and obesity-associated

protein (FTO) and AlkB Homolog 5, RNA Demethylase (ALK5B)[6,7]. A variety of reader proteins in different subcellular localizations recognize m6A and mediate m6A's regulatory function on mRNA metabolism. Established functions of m6A include promoting transcript decay (e.g. by YTH domain-containing family protein 2 (YTHDF2)); transcript stability (e.g. by insulin-like growth factor mRNA-binding proteins (IGF2BPs) and Leucine rich pentatricopeptide repeat containing (LRPPRC)), translation (e.g. by YTH domain-containing family protein 1 (YTHDF1) and Eukaryotic initiation factor 3 (eIF3)), splicing (e.g. by YTH N6-Methyladenosine RNA Binding Protein C1 (YTHDC1) and Heterogeneous nuclear ribonucleoproteins A2/B1 (HNRNPA2B1)), and nuclear export by YTHDC1, among others[8–16]. Finally, recent studies note the role of m6A in preventing formation of anomalous double stranded RNA (dsRNA) structures and their recognition by innate immune sensors[17,18].

Similar to METTL3, adenosine deaminases acting on RNA-1 (ADAR1) also modify adenosine bases by deaminating A to inosine (I) in the context of dsRNA[19]. Inosine pairs preferentially with cytosine and therefore is decoded as Guanosine by the cell translational machinery[20]. Two different ADAR1 isoforms exist, the constitutively expressed (and mostly nuclear) p110 isoform and the interferon-induced (and mostly cytoplasmic) p150 isoform which has important roles in the antiviral responses. A-to-I editing occurs most frequently in repetitive elements such as short interspersed nuclear elements (SINE), introns, and the 3'UTR, due to their propensity to form dsRNA structures[20]. ADAR1 editing and binding of such dsRNA structures prevents activation of innate immune sensing pathways[21,22].

Both m6A and A-to-I RNA editing target adenosine, suggesting a potential for interactions. While several studies have investigated each modification independently, questions regarding their interplay remain unresolved, in part due to conflicting data. For example, in the context of breast cancer, ADAR1 appears to increase METTL3 abundance as well as m6A levels, through the editing of the 3'UTR of *METTL3* that alters a miRNA binding site[23]. Conversely, through studies in glioblastoma, METTL3 was found to directly methylate *ADAR1* mRNA[24]. More broadly, some studies reported a negative correlation between A-to-I editing and m6A but increased A-to-I editing upon METTL3 deletion on m6A-depleted

transcripts. Interestingly, in a subset of transcripts, methylation was accompanied by increased A-to-I editing levels, yet, this subset of transcripts was not further examined[25].

To explore the dynamics and possible relationship of m6A and A-to-I RNA modification events we have focused on macrophages, for three reasons: first, because macrophages readily adapt their phenotype and function, in response to changes in tissue physiology and external stimuli. This means that we can match changes in modification events to specific (and well understood) functional outputs, from the upregulation of activation markers to the phagocytic ability of cells proficient or deficient in modification enzymes. Second, there have already been studies that link specific modification events to key functions, which we can use as benchmarks in our analyses. For example, m6A was reported to positively regulate macrophage activation by stabilization of Signal transducer and activator of transcription 1 (*STAT1*) mRNA; METTL3 was shown to increase phagocytosis capacities[26] and to regulate the inflammatory response in macrophages through nuclear factor kappa-light-chain-enhancer (NF-κB) signaling, possibly by *TRAF6* mRNA methylation[27,28]. Similarly, ADAR1 was found to promote macrophage activation through NF-κB signaling[29], and lack of ADAR1 was shown to inhibit NF-κB signaling as well as downstream inflammation mediators like inducible nitric oxide synthase (NOS2) and interleukin-1β (IL1b)[30]. Thus, it is clear that m6A and A-to-I deamination independently function in the regulation of macrophage activity. And third, macrophage cell lines (like the RAW cells we use here) have been used in the past for studies on RNA processing[31], which means that possible interdependencies between modifications can be assessed mechanistically. Here, starting with RAW cells proficient or deficient for METTL3 or ADAR1, and using Nanopore direct RNA sequencing, Illumina sequencing and orthogonal validation assays, we identify interdependencies between these two modifications and show their relevance to RNA therapeutics.

Results

The response of naive RAW 264.7 macrophages to pro-inflammatory stimulation by combined LPS and IFN-γ treatment. A-to-I and m6A RNA modifications overlap in their distribution along the gene body, as both modifications commonly occur within the 3′UTR[2,5,20]. This proximity suggests a potential interplay

between the two types of adenosine modifications. Moreover, in independent studies, m6A and A-to-I editing were found to regulate macrophage activation[26–30,32], raising the question if the RNA modifications also influence each other and cooperatively facilitate the pro-inflammatory phenotype of macrophages. To investigate their dynamics and possible functional relationship during macrophage activation, we employed the murine RAW 264.7 (RAW) macrophage cell line as a model for monocyte-derived macrophages. Upon stimulation with lipopolysaccharide (LPS) and interferon (IFN)-γ, RNA was extracted at regular time intervals and examined by Illumina Next Generation Sequencing (NGS) (Fig. 1A). In line with previous observations, we detected rapid transcriptional changes characteristic of pro-inflammatory macrophage activation (GO:0042116), with key genes upregulated as early as 2 hours post-stimulation (Fig. 1B). Distinct temporal expression patterns emerged, underscoring the dynamic nature of this response. Genes encoding for pro-inflammatory cytokines such as Tumor necrosis factor (*Tnf*) and Interferon-β1 (*Ifnb1*), which are typically expressed at low levels under basal conditions, showed a marked increase in expression beginning at 2 hours. In contrast, genes with negligible basal expression, including Toll-like-receptors (*Tlrs*) which are involved in recognizing pathogen associated molecular patterns[33], e.g., *Tlr1*, *Tlr6*, *Tlr3*, and *Tlr9*, exhibited robust induction at 12 hours. Meanwhile, a group of genes that is constitutively expressed in resting macrophages demonstrated phased downregulation at various stages after stimulation, as observed for *Il1rl1*, *Cahlm2*, *Cebpa*, *Cx3cr1* and *Trem2*. These temporal patterns are more clearly illustrated in the bar plot of log fold-change (LogFC), ordered by the magnitude of change and progressing from 2 to 24 hours (top to bottom, Fig. 1C).

Loss of METTL3 from RAW macrophages affects A-to-I editing levels. To assess potential interactions between m6A and adenosine deamination, we generated clonal cell lines lacking either the A-to-I editing enzyme ADAR1 or METTL3, the catalytic subunit of the m6A writer complex (SupplFig. 1A-D, SupplFig. 2A-D). Currently, ONT algorithms are unable to detect A-to-I editing (A-to-I) (SupplFig. 2F). Therefore, we opted to use the well-established Illumina sequencing platform to investigate ADAR1 dependent RNA editing events during macrophage activation, as well as to examine how these processes are influenced by

the absence of METTL3. As the ADAR1 p150 isoform is interferon inducible, we expected increased levels of ADAR1 expression upon LPS and IFN-γ treatment. Indeed, both control (Ctrl) and METTL3-KO cells exhibited an upregulation of *Adar1* mRNA already at 2 hours post-stimulation, which continued to increase at later time points (Fig. 2A). No significant differences in *Adar1* mRNA expression were observed between the two groups after stimulation. However, at steady state, *Adar1* transcript levels are slightly higher in METTL3-KO (a ~2-fold increase) compared to control conditions (SupplFig. 1E). Protein levels followed a similar trend, albeit with a delay, as increases in ADAR1 protein were detectable only at 12 and 24 hours post-stimulation. Moreover, METTL3-KO macrophages showed a delay in ADAR1 protein upregulation in response to stimulation as seen in lower ADAR1 protein levels at 12 hours, while ADAR1 levels after 24 hours were equal between METTL3-KO and control conditions (Fig. 2B–C).

In parallel, we investigated changes in global A-to-I RNA editing across conditions. Upon inflammatory stimulation, the number of editing sites increased in parallel with ADAR1 levels, peaking at 24 hours. There were no substantial differences in global editing events between control and METTL3-KO macrophages (Fig. 2D, SupplFig. 1F). In control conditions, a large proportion of editing sites exhibited increased levels of editing upon stimulation, starting from 12 hours (data not shown) and progressing further at 24 hours (Fig. 2E, SupplFiles-Table-1). The mean editing levels at these sites increased significantly, rising from approximately 10 % in unstimulated macrophages to around 25 % after stimulation (SupplFig. 1H left). Both observations highlight a clear editing response to inflammation. A similar effect was observed in the METTL3-KO macrophages regarding the number of editing events, while mean editing levels in stimulated METTL3-KO macrophages were approximately 18 %, hence, slightly lower as compared to control macrophages (SupplFig. 1H right 1I). Differential editing analysis in unstimulated macrophages revealed that only 8 sites exhibited higher editing levels in control than in METTL3-KO cells, while 12 sites displayed reduced editing levels in control cells (Fig. 2F, SupplFiles-Table-2). However, the situation changed 24 hours post-stimulation, with many editing sites exhibiting reduced editing levels in the METTL3-KO macrophages (Fig. 2G, SupplFig. 1I, SupplFiles-Table-3). Overall, our data demonstrate that the loss of

METTL3-dependent m6A methylation leads to a global reduction in A-to-I RNA editing levels suggesting a functional interplay between m6A modifications and ADAR1 activity.

Loss of ADAR1 from RAW macrophages does not interfere with m6A levels. Next, we focused on clonal RAW cell lines lacking the A-to-I editing enzyme ADAR1 to examine how its loss might affect METTL3 dependent m6A deposition. Mettl3 mRNA levels were similar in unstimulated control and ADAR1-KO RAW macrophages (Fig. 3A). However, higher Mettl3 mRNA levels were detected at 12 and 24 hours post-stimulation in ADAR1-KO compared to control cells (SupplFig. 2E). While the unstimulated control cells expressed slightly more METTL3 protein as compared to the ADAR1-KO cells, this difference was no longer observed upon stimulation, where METTL3 protein expression was found to be largely stable and independent of ADAR1 (Fig. 3B-C).

We then employed Oxford Nanopore direct RNA sequencing to investigate the status of m6A modifications. Given that the most significant increases in RNA editing and major changes in gene expression were identified after 24 hours, we sequenced the RNA only from unstimulated macrophages and 24 hours post-stimulation. To identify METTL3-dependent m6A sites, we performed differential methylation analysis, revealing candidate positions with loss of methylation in METTL3-KO compared to controls, while filtering out unchanged sites to minimize false positives (see Methods for details on filtering criteria, SupplFig. 2F-G). We further confirmed that the majority of m6A sites identified by our bioinformatic pipeline were located within the consensus DRACH motif (Fig. 3D-E). The global number of m6A sites appeared unaffected by inflammatory stimulation in the control condition. However, a reduction in global m6A sites was observed in ADAR1-KO cells 24 hours after stimulation compared to their resting state (Fig. 3F). As m6A's importance in macrophage activation has been described in the past [26–28], we further investigated whether this was reflected by changes in m6A frequency per modified site. We found that only very few sites were differentially methylated during the inflammatory response (Fig. 3G, SupplFiles-Table 4-5). Additionally, m6A sites exhibit nearly identical methylation levels between control and ADAR1-KO macrophages, both before and after pro-inflammatory stimulation, with only a few exceptions (Fig. 3H-I). In summary, these data show that global ADAR1 depletion does not affect m6A deposition or levels.

Impact of adenosine modifications on macrophage activation. After identifying global changes in m6A and A-to-I modifications upon pro-inflammatory stimulation, we focused on the impact of the mRNA modifications on macrophage function. As both RNA modifications have been independently implicated in preventing aberrant dsRNA formation and innate immune activation[17,18,21,22], we investigated the induction of an interferon response upon the loss of each modification. We detected downregulation of several interferon stimulated genes (ISG) in ADAR1-KO macrophages (SupplFig. 3C-D); this is surprising only when considering the published literature which clearly shows that loss of ADAR1 leads to inflammation through ISG upregulation[21,22,34,35]. However, it is worth noting that loss of ADAR1 also from other immune cell types (e.g. B cells[34], Natural Killer cells – unpublished observation) rather leads to a phenotype where the ISG response is dampened rather than stimulated. In contrast, several type-I interferon induced genes were upregulated in METTL3-KO macrophages in comparison to control macrophages in the absence of external stimulation (Fig. 4A). Additionally, many genes involved in the dsRNA response were upregulated in METTL3-KO macrophages (Fig. 4B), further supporting the role of m6A in preventing endogenous aberrant dsRNA formation[17,18]. Likewise, remarkable differences in expression of interferon and dsRNA response genes were observed between control and METTL3-KO cells 24 hours after LPS and IFN-γ treatment, suggesting that ISG expression is regulated by m6A (indicated by the presence of m6A in many differentially expressed transcripts; Fig. 4A-B) and/or by the upregulation of m6A readers (*Igf2bp1*, *Igf2bp2*, and *Lrpprc*) during stimulation (SupplFig. 3E-G). We observed RNA editing events and m6A sites in multiple transcripts associated with macrophage activation (Fig. 4C), raising the question of whether these modifications directly contribute to macrophage activation.

As noted earlier, LPS and IFN-γ treatment led to transcriptional upregulation of a variety of macrophage activation markers and inflammatory cytokines, many of which showed changes in expression in the absence of ADAR1 or METTL3 (Fig. 4D, SupplFig. 3A-B). To assess, if transcriptomic changes were also reflected on the protein level, we measured the cell surface expression of proteins required for macrophage activation by flow cytometry (Fig. 4E). Upon stimulation, control macrophages displayed

increased expression of cell surface proteins typically associated with M1 polarization, including MHC II, CD80, CD40, and β2M (required for MHC I presentation). While the expression of these proteins was only mildly affected by ADAR1-KO, METTL3-KO macrophages showed a strong deficiency in upregulation of these surface proteins, most pronounced for MHC II and CD80 (Fig. 4F). Notably, these molecules play an important role in antigen presentation and co-stimulation of a T cell response, hence facilitating the communication between macrophages and the adaptive immune system to elicit an adequate immune response[36]. As well, the scavenger receptor CD36 failed to be upregulated in METTL3 KO macrophages during pro-inflammatory stimulation (Fig. 4G). Interestingly, when investigating TLR2, which is involved in the recognition of different pathogen associated molecular patterns (PAMPs) and the induction of phagocytosis, we observed increased expression in resting METTL3-KO cells as compared to control or ADAR1-KO cells, while the levels of TLR2 were not different between the genotypes after pro-inflammatory stimulation (Fig. 4G).

Impact of adenosine modifications on phagocytosis. As we observed pronounced changes in the expression of surface receptors that mediate phagocytosis as a key macrophage function, we asked whether phagocytosis activity would be affected by loss of ADAR1 or METTL3. Interestingly, many mRNAs encoding proteins related to phagocytosis were not only induced upon LPS and IFN-γ treatment, but also contained m6A sites, A-to-I editing sites or both (Fig. 5A). Moreover, the expression of many of these genes was deregulated in the absence of ADAR1 or METTL3 (Fig. 5A-B). To functionally test whether adenosine modifications impact phagocytosis, resting macrophages were incubated with particles containing a pH-sensitive green fluorophore (pHrodo Green) and conjugated with either *Staphylococcus aureus* (*S. aureus*) or the yeast cell wall component zymosan. In the acidic environment of the endosome, endocytosed particles would emit fluorescent signals, thus allowing quantification by flow cytometry (Fig. 5C). In unstimulated conditions, an equal number of control and ADAR1-KO cells phagocytosed *S. aureus* particles, while the uptake of *S. aureus* per phagocytosing cell was slightly higher in ADAR1-KO macrophages. Untreated METTL3-KO cells showed a pronounced increase in both the percentage of

phagocytosing cells and in the number of *S. aureus* particles taken up per cell (Fig. 5D), possibly due to their priming by the ISG response as described above (Fig. 4A). In contrast, the cells' capacity to take up zymosan particles was decreased in the absence of METTL3 while it was not affected by ADAR1 loss (Fig. 5E).

As surface marker expression indicated impaired activation of METTL3-KO macrophages after pro-inflammatory stimulation (Fig. 4F-G), we wanted to test if this was accompanied by attenuated phagocytosis activity. Hence, we repeated the phagocytosis assay with macrophages pre-stimulated for 24 hours with LPS and IFN-γ. Interestingly, pre-stimulated METTL3-KO and ADAR1-KO cells took up significantly lower amounts of *S. aureus* particles per cell as compared to control cells (Fig. 5F). Also the uptake of zymosan particles was strongly reduced in both KOs as compared to control macrophages under this experimental condition (Fig. 5G). Together, these findings indicate that phagocytosis is affected by loss of either METTL3 or ADAR1. Observing differences in uptake of *S. aureus* and zymosan between the different genotypes, likely reflects that METTL3 and ADAR1 regulate distinct receptors and pathways mediating ligand recognition and phagocytosis. Further, the role of RNA modifiers in controlling phagocytosis capacity appears to be different in resting and stimulated macrophages.

Interdependencies between m6A and A-to-I modifications. To begin to assess a direct interplay between the two adenosine modifications, we first asked whether the reduction of A-to-I editing in stimulated METTL3-KO macrophages (Fig. 2G) was solely due to reduced ADAR1 protein expression, which in turn might be attributed to m6A sites on the *Adar1* transcript (a set of which was previously identified[24]). Examination of our dataset confirmed the presence of several m6A sites within the last exon and 3'UTR (SupplFig. 4A), which have been proposed to play a role in the translation of ADAR1[24]. Furthermore, ribosome profiling suggested that *Adar1* translation efficiency is reduced in the METTL3-KO cells after pro-inflammatory stimulation (SupplFig. 4B). However, the minor reduction in ADAR1 protein production in the METTL3-KO macrophages was only observed at 12 hours post-stimulation with protein abundance increasing at later points (Fig. 2B-C). Thus, ADAR1 protein levels alone are likely not the reason

for the loss of A-to-I editing that we observe 24 hours after stimulation. Moreover, our data reveal a second cluster of m6A sites within the second *Adar1* exon. m6A sites within exons have been reported to affect splicing [12,15]) and so we asked whether loss of m6A would affect the splicing of *Adar1*. Indeed, we found an increased ratio of poly-adenylated mis-spliced over correctly spliced *Adar1* transcripts in the METTL3-KO cells as compared to control cells particularly after stimulation (SupplFig. 4A, C-D). However, again, none of these effects of m6A on the *Adar1* transcript appeared to lead to significant amounts of altered ADAR1 protein. Therefore, the global dependency of A-to-I levels on m6A that we observe is not the indirect outcome of effects of m6A on the *Adar* transcript.

We then turned our attention to more direct effects that would suggest an interaction between A-to-I editing and sites of m6A methylation, and assessed the prevalence of the two modifications across expressed genes in control macrophages 24 hours after LPS and IFN-γ treatment (where m6A and high A-to-I editing levels were observed). Among the approximately 12,000 genes with detectable expression, more than half contained at least one modification site. Specifically, 2.8 % of these genes exhibited only A-to-I editing sites, 11 % had both m6A and A-to-I sites, and 45 % displayed only m6A sites. The remaining 40 % of genes appeared to be free of these two RNA modifications (Fig. 6A). Interestingly, genes decorated with both RNA modifications are among the most highly expressed across all conditions, suggesting that detection of modifications may be biased toward higher-expressed transcripts (Fig. 6B, SupplFig. 4E). Although METTL3 and ADAR1 are thought to target different RNA substrates — with METTL3 acting on single-stranded RNA (ssRNA, preferentially at canonical DRACH motifs) and ADAR1 on dsRNA, both enzymes target overlapping genic regions. Overall, we observed modification enrichment around the Transcription start site (TSS), 5’ UTR, 3’ UTR, and TTS, suggesting potential regulatory roles at these regions (Fig. 6C).

Current Nanopore basecaller models that are meant to detect A-to-I editing, are not reliably able to identify differences in A-to-I levels between ADAR1-KO and control cells (SupplFig. 2F left), preventing simultaneous detection of the two RNA modifications on the single transcript level. As an alternative, we analyzed the frequency of both modifications in relation to their distance in control macrophages by

combining modified sites identified from Illumina (for I) and Nanopore sequencing (for m6A, Fig. 6D). These analyses revealed that A-to-I editing and m6A modifications can occur in close proximity, particularly within the 3' UTR and TTS. Specifically, we identified 220 genes where 350 A-to-I editing sites were located within 50 nucleotides of 246 m6A sites (Fig. 6D). Interestingly, this proximity was only observed when both modifications occurred on the same RNA strand (in cis). When analyzing distances between modifications on sense and its anti-sense strand strands—i.e., in trans, (which can occur when both sense and antisense RNAs are expressed) —this proximity effect was not detected.

To further investigate the potential interaction between the two modifications, we interrogated the data from control macrophages treated for 24 hours with LPS and IFN-γ, as both the number of editing sites and their cumulative abundance increased upon stimulation. The distance between modifications was ranked using quantiles (Q), and categorizing as close (Q1), medium (Q2), or far (Q3) (Fig. 6D). We examined the editing frequencies at different m6A modification levels, as well as A-to-I/m6A. Our analysis shows that editing frequency could be influenced by m6A modifications, with a weak decreasing association when the two modifications are in close proximity (<139 nt, Q1: close), particularly at highly methylated m6A sites (Fig. 6E upper panel, SupplFig. 4G). For editing sites located at medium (139–1192 nt, Q2: medium, Fig. 6E upper) or high distances (>1192–10,000 nt, Q3: far, Fig. 6E upper panel) from m6A sites, there is an increase in editing frequencies associated with higher m6A levels (Fig. 6E bottom figure, SupplFig. 4G). However, in RNA from METTL3-KO cells (lacking m6A), the editing frequencies are lower, regardless of the proximity of the relevant methylation site, pointing to a more global effect (Fig. 6F). These observations were further supported by a multivariate regression model (see SupplTable 1 for model details).

The association between m6A levels and A-to-I editing frequency at distant sites suggests a role for m6A in the recruitment of ADAR1 on the transcript either through means of common interacting proteins (for example interactions between m6A readers and ADAR1 itself[37]) or through RNA-structural means (for example a stabilization of a labile dsRNA intermediate through m6A deposition[17]). To assess the second possibility, we took advantage of an artificial reporter system that reports on A-to-I editing efficiency through

the recruitment of endogenous ADAR1 to the mRNA coding an eGFP-mutant where a tryptophan codon (UGG) is mutated to a stop codon UAG (stop) codon at position 58 (W58X) producing truncated non-fluorescent eGFP. ADAR1 editing at this specific location reverts the mutation at the RNA level and leads to eGFP expression. Therefore, gRNA-dependent ADAR1-recruitment can be easily measured with flow cytometry[38]. Recruitment is achieved by provision of antisense RNA oligos (ASOs or ADAR engagers)[38,39] to facilitate site-specific editing at the adenosine of the internal UAG stop codon, yielding UIG (decoded as UGG- tryptophan) and allowing for the production of eGFP (Fig. 6G). To test whether m6A could have a direct impact on ADAR1 recruitment we delivered in-vitro transcribed ASOs where all adenosines were substituted with m6As. Surprisingly, ASOs containing m6A increased ADAR1 recruitment more than 4-fold at various time points measured as eGFP reactivation in flow cytometry (Fig. 6H). Aside from their serendipitous relevance in the field of RNA therapeutics, these results support the notion that m6A can act "at distance" to increase ADAR1 engagement in cis, resulting in increased A-to-I editing.

Discussion

Macrophage cells exemplify remarkable plasticity. These cells must respond to a diverse array of stimuli to maintain tissue homeostasis and defend against a multitude of threats. Achieving this requires highly orchestrated, well-regulated, and rapid responses that extend beyond direct transcriptional and translational changes, incorporating modulation of the epitranscriptome. This additional layer of regulation enables a faster and more adaptive response, shaping macrophage behavior and guiding these cells into specific activation states. These activation states are not confined to the extremes of M1 (pro-inflammatory) and M2 (anti-inflammatory) polarization, but instead represent a continuum of specialized functions tailored to meet specific environmental and physiological demands. This versatility equips macrophages with precision and efficiency in performing their roles, underscoring their importance in immune regulation and tissue repair.

The pro-inflammatory stimulus represented by LPS and IFN-γ treatment mimics an M1 activation response - and as we and others have shown, this response is temporally dynamic: it is characterized by

the early induction of genes such as *Ifnb1* and *Tnf* (among many other LPS-responsive genes, Fig. 1B-C) that are rapidly activated through the promotion of transcription elongation from a poised transcription initiation complex, ensuring a rapid onset of the response[40,41]. These gene products then orchestrate the activation of downstream intermediate and late response genes to elicit a comprehensive inflammatory response (Fig. 1B-C)[42], which also involves induction of negative feedback loops through translational regulation of specific mRNAs [31] .

Here, we have identified m6A and A-to-I RNA editing sites in several genes involved in macrophage activation and in key functions such as phagocytosis (Fig. 4C, Fig. 5A). We also demonstrated that loss of these RNA modifications leads to impaired macrophage activation and phagocytosis upon pro-inflammatory stimulation (Fig. 4F–G, Fig. 5D–G), underlining the crucial role of RNA modifications in rapidly responding to specific cues. Specifically, we and others have observed a defining role of m6A in macrophage activation[26–28,32]. However, we did not observe major changes in RNA methylation in response to pro-inflammatory stimulation (Fig. 3G), despite the substantial gene expression changes during the response which also includes differential expression of many methylated transcripts (Fig. 4C). This reflects, not m6A abundance changes upon macrophage activation but rather its recognition by m6A reader proteins, which regulate RNA metabolism [16] and, thereby, lead to functional modulations[43,44]. Interestingly, we and others have observed expression changes in several m6A readers, particularly *Igf2bp1*, *Igf2bp2*, and *Lrpprc*, upon inflammatory stimulation, which may underlie the functional importance of m6A modification during macrophage (SupplFig. 3G)[32].

In line with previous observations, ADAR1 deaminase activity increases after macrophage stimulation, accompanied by a global increase in the number of editing sites, which follows the rise in protein levels in both control and METTL3-KO cells, with minor differences observed between the two genotypes. Another measure of editing activity, the global frequency of editing events per site, is strongly induced by LPS and IFN-γ, as shown in Fig. 2E. Interestingly, no differential editing is observed between control and METTL3-KO cells in unstimulated conditions, yet many editing sites (belonging to approximately 300 genes) exhibit lower editing levels in METTL3-KO macrophages upon stimulation (Fig. 2G). These

results suggest a positive impact of m6a on A-to-I editing frequencies, indicating that ADAR1 may edit more efficiently in the presence of m6A.

Based on the dataset from control macrophages, we found that 11 % of transcripts are both edited and methylated (Fig. 6A). Because the Nanopore base-calling model was unable to reliably detect inosine at the time of our analysis (SupplFig. 2F), we combined m6A sites identified by Nanopore sequencing data with inosine occurrences determined by Illumina short read sequencing. Cross-referencing data from different sequencing techniques is a limitation as it does not allow us to determine whether m6A and A-to-I modifications truly co-occur within the same transcript. Instead, we opted for assessing the potential co-regulation of the two modifications as a function of their distance between each other (Fig. 6D), and asked whether a distance-dependent interaction occurs when the modifications are in close proximity. By doing so we found a mild negative association of A-to-I with sites of high m6A levels at close distances (< 139 nt) within a transcript (Fig. 6E). This is in line with expectations for the following reasons: (i) once an adenosine is deaminated, it can no longer be methylated—and vice versa—when the two modifications overlap at the same site (Direct Modification Competition)[45]; (ii) the two modifications target distinct substrates (double-stranded RNA for A-to-I editing and single-stranded RNA for m6A methylation,), and exhibit different binding preferences (AU-rich regions for A-to-I editing and DRACH motifs for m6A[3,46]) (Distinct Structural Requirements), and (iii) competition between ADAR1 and m6A-reader proteins for RNA binding—and vice versa (Protein-Mediated Competition).

In contrast, we found a strong association at medium and far distances (≥139 nt), where high m6A levels positively correlated with A-to-I editing sites (Fig. 6E). This was surprising and suggested either (i) a structural relationship where a m6A modification affects a distal (≥139 nt) ADAR1 A-to-I editing site through RNA looping or folding (Structural RNA Interactions (Long-Range Effects))[47,48] or (ii) a protein interaction-mediated relationship where m6A reader proteins at a distal site can help recruit ADAR1 to deaminate its target transcript (Protein-Mediated Recruitment)[37], or both.

To test the first hypothesis, we artificially recreated a dsRNA structure to recruit endogenous ADAR1 with m6A on the ADAR-recruiting guide (an artificially synthesized oligo strand) opposite to the target A-to-I

site. Editing of the target site allows restoration of eGFP expression which could be easily measured by the number of green fluorescent cells. To test a possible effect from m6A on ADAR1 editing in these settings, we delivered gRNAs with or without m6A substitution (Fig. 6G). Surprisingly, methylation of the guide consistently led to substantially higher levels of ADAR1-dependent A-to-I editing on the Egfp transcript, and therefore higher levels of eGFP expression (Fig. 6H). Together, these findings suggest a potential structural interaction between m6A and A-to-I sites at a distance. Given the recent developments of using guided ADAR1 editing for novel therapeutic approaches[49,50], incorporating m6A into guide RNAs may be instrumental to increasing therapeutic editing levels.

Finally, our findings provide a novel mechanistic link between m6A and A-to-I editing, suggesting that m6A modifications may play a broader role in regulating ADAR1-mediated RNA editing in a subset of transcripts through at least 5 different, non-mutually exclusive mechanisms: (i) Direct modification competition; (ii) Distinct structural requirements; (iii) Protein-mediated competition; (iv) Structural RNA interactions (long-range effects); and (v) Protein-mediated recruitment. This interplay could have significant implications for understanding RNA modification dynamics and their functional impact on transcriptome plasticity. Future research should aim to determine whether this effect is conserved across different cellular contexts, tissue types, and physiological conditions. Additionally, it will be interesting to explore the molecular mechanisms underlying this interaction and assess how it can be leveraged to enhance the efficiency and specificity of targeted RNA therapies.

Materials and Methods

Cell culture

RAW 264.7 (RAW) macrophages were cultured in cell-culture treated vessels in DMEM (high glucose) supplemented with 10 % FCS, 1 % L-glutamine, and 1 % penicillin/streptomycin at 37 °C, 5 % CO2, and relative humidity 90 %. For M1 polarization, cells were stimulated with 100 ng/ml LPS and 20 ng/ml IFN-y for indicated durations. HEK293T cells (obtained from DKFZ, ATCC, Cat# CRL-3216, RRID: CVCL_0063) were cultured at 37°C, 5% CO2 in high-glucose DMEM (Sigma-Aldrich, Cat# D6429) supplemented with 10% FBS (PAN Biotech, Cat# P40-37100) and 1% penicillin/streptomycin (Sigma-Aldrich, Cat# P4333). The cell line was authenticated using Multiplex Cell Authentication by Multiplexion (Heidelberg, Germany). Additionally, the purity of both cell lines was validated using the Multiplex cell Contamination Test by Multiplexion (Heidelberg, Germany). No Mycoplasma, SMRV, or interspecies contamination was detected.

Generation of RAW knockout and control cell lines

Guides targeting the genomic sequence of METTL3 (exon 1: GCGAGAGATTGCAGCGGCGA, exon 3: GGGCGGCAAATTTCTGGAGA), and Adar1 (exon 2: ACTCTAACAACCCGCTGACA), as well as non-targeting control guides (GCTTTCACGGAGGTTCGACG, ATGTTGCAGTTCGGCTCGAT) were cloned into plasmid pSpCas9(BB)-2A-GFP (PX458, Addgene, #48138, a gift from Feng Zhang). RAW cells were nucleofected with plasmids using Amaxa's Cell Line Nucleofector Kit V (Lonza, 10507935) and the manufacturer's protocol for Nucleofector II Device. 48 h after nucleofection, cells were resuspended in cell sorting buffer (PBS supplemented with 2 % FCS, 25 mM HEPES, and 2 mM EDTA), stained with Propidium iodide (Invitrogen, BMS500PI) for live/dead discrimination and GFP expressing clones were single-cell sorted for ADAR1 and METTL3 KO clones and sorted in bulk for the non-targeted control on the BDAria 3 Cell Sorter.

Validation of KO cell lines

After expansion, clonal cell lines were screened for biallelic indels by amplification of the targeted gene region by polymerase chain reaction (PCR) using Q5 high-fidelity DNA polymerase (NEB, M0491L) with associated reagents according to NEB's standard protocol and Sanger Sequencing. Knockouts were confirmed on the protein level using Western blot. For METTL3 KO clones, transcript isoforms regulated by m6A mRNA modification were quantified by reverse-transcription quantitative PCR (RT-qPCR) as described below.

Flow cytometric analysis of cell surface markers

Unstimulated or cells stimulated for 24h with 100 ng/ml LPS and 20 µg/ml IFNγ were harvested in FACS buffer (PBS supplemented with 2 % FCS), incubated for 10 minutes in homemade Fc blocking buffer, stained for 30 minutes with antibody staining cocktail in FACS buffer, followed by 30 min staining with violet live/dead fixable staining solution (Invitrogen, 34964, 1:1000 in PBS), and fixation for 10 minutes with 4 % Paraformaldehyde (Thermo, 28908) in PBS. Between steps, cells were washed by adding an excess FACS buffer and centrifugation for 5 minutes at 800 g at 4°C. Samples were analyzed using the BD Canto II flow cytometer. Antibodies used: CD40 APC/fire, Biolegend, 124632; CD36 APC, Biolegend, 102611; I-A/I-E FITC, Biolegend, 107605; APC anti-mouse β2-microglobulin, Biolegend, 154505; H-2 PE, Biolegend, 125505; CD80 PE, BD, 553769).

Phagocytosis assay

For unstimulated samples, 100 000 cells were plated in flat-bottom 96-well plates in fresh medium and allowed to attach for 1 h. For stimulated samples, 10 000 cells were plated two days before phagocytosis assay and treated for 24h with 100 ng/ml LPS and 20 µg/ml IFNγ. Cells were washed twice with non-supplemented DMEM (high glucose), followed by adding 5 µg pHrodo Green S. aureus (Invitrogen, P35367) or Zymosan (Invitrogen, P35365) particles in 50 µl non-supplemented DMEM. Cells were incubated with particles for uptake for 1 h at 37°C. Cells were harvested, incubated for 30 minutes with violet live/dead fixable staining solution (1:1000 in PBS), and washed. Cells were analyzed at the BD Cytek Aurora Spectral Flow Cytometer using automated spectral unmixing.

Next Generation Illumina Sequencing (NGS)

For NGS sequencing, RNA extraction was performed using the RNeasy Mini kit (Qiagen, 74104) according to the manufacturer. Contaminating DNA was removed using the Turbo DNase-free Kit (Invitrogen, AM1907) according to the manufacturer. RNA was quantified by Nanodrop and submitted to the DKFZ Core Facility for library preparation (rRNA depletion protocol) and sequenced using NovaSeq 6000 Sequencing System (Illumina).

Direct RNA sequencing using Oxford Nanopore Technology

Unstimulated and cells treated for 24 h with LPS and IFN-y treatment were lysed in Trizol and RNA was extracted using Zymo Direct-Zol Kit (Zymo, R2050) including DNase I treatment. Libraries were prepared from 2.5 µg total RNA using the Direct RNA Sequencing Kit (SQK-RNA004) according to the manufacturer. Libraries were loaded on the PromethION RNA Flow Cell (FLO-PRO004RA) on the promethION 24 sequencing device.

RNA LC-MS/MS

Unstimulated and cells treated for 24 h with LPS and IFN-y treatment were lysed in Trizol and RNA was extracted using Zymo Direct-Zol Kit (Zymo, R2050) including DNase I treatment. Poly-A enrichment was performed using the NEBNext Poly(A) mRNA Magnetic Isolation Module (NEB). RNA samples from three replicates were pooled and RNA was precipitated overnight at -70°C using ammonium acetate (Sigma, A2706) and ice-cold ethanol. RNA was digested and internal standards of 13C labeled yeast RNA was added. Calibration samples of unmodified and modified nucleotides were prepared. Samples were injected into the LC-MS/MS instrument for measurement. Data was analyzed using the Aligent Masshunter qualitative and quantitative software.

Reverse transcription (RT) and RT qPCR

RNA extraction for downstream reverse transcription was performed using the RNeasy Mini kit (Qiagen, 74104) according to the manufacturer. Contaminating DNA was removed using the Turbo DNase-freeKit (Invitrogen, AM1907) according to the manufacturer. Reverse transcription was performed using ProtoScript First Strand cDNA Synthesis Kit (NEB, E6300L) according to the manufacturer. Quantitative PCR, was performed using iTaq Universal SYBR Green Supermix (Biorad, 1725121) according to the manufacturer using the CFX Connect Real-Time System (Bio-Rad). Samples were normalized by the amount of the housekeeper CPH (CPH_fw: ATGGTCAACCCCACCGTG ; CPH_rv: TTCTTGCTGTCTTTGGAACTTTGTC) present in each sample. Oligos used to target transcripts: Tor1aip2_long_ex-junction_fw: TCTGGACCTATGGTTCCGTG; Tor1aip2_long_ex-junction_rv: GCTGGGCTGGGGAAGAATAG; tor1aip2_short_ex3_fw: TGGGTCTGCTTCTGTGGTCT; tor1aip2_short_ex3_rv: CAAGAGGGGCCAGGTAGTTC; Adar1_ex2_fw: GATGCCCTCCTTCTACAGCC; Adar1_ex3_rv: ATTCCCGCCCATTGATGACA; Adar1_in2-3_rv: TCTGGGCAGTCTCTTACCGA.

Western blot

Cultured cells were washed with PBS and lysed in Cell Lysis Buffer (Cell signaling, 9803) containing cOmplete, Mini, EDTA-free Protease Inhibitor Cocktail (Roche, 11836170001) and 1 mM phenylmethylsulfonylfluoride (Sigma, 93482, 1:100) for 30 minutes on ice, followed by centrifugation for 15 min at 10 000 g at 4 °C. The protein in the supernatant was quantified using the Pierce BCA Protein Assay Kit (Thermo, 23225) according to the manufacturer, and was cooked with Laemmli buffer for 5 minutes at 95 °C. Samples were loaded on Mini-PROTEAN TGX Precast Gels (4-15%, Bio-Rad, 4561086) and run for 30 minutes at 70 V followed by 130 V until reaching desired separation. Proteins were transferred to a

Nitrocellulose Blotting Membrane (Cytiva) using a wet blotting system for 70 minutes at 100 V. The nitrocellulose membrane was blocked for 1 h with 5 % skim milk in TBS-T (1X TBS with 0.1 % Tween-20). Membranes were incubated with primary antibodies (METTL3, Abcam, ab195352; ADAR 1, Santa cruz, sc-73408, beta-actin, Sigma, A5441; alpha Tubulin, Abcam, ab4074) in 5 % milk - TBS-T overnight at 4 °C while rotating. Membranes were washed three times with TBS-T and incubated with corresponding horseradish peroxidase-coupled secondary antibodies (goat anti mouse - HRP (H+L), Biorad, 170-6516; goat anti rabbit-HRP (H+L), Biorad, 170-6515) in 5 % skim milk - TBS-T for 1 h at
room temperature while shaking. After three washes with TBS-T, membranes were incubated with chemiluminescence based detection reagent 1 and 2 at equal volumes (ECL Start Western Blotting Detection Reagent, Cytiva, RPN3243, or SuperSignal West Pico PLUS Chemiluminescent Substrate, Thermo, 34095). Chemiluminescent signals were detected using the ChemiDoc Imaging System (BioRad). Densiometric quantification was performed using the ImageG software. Amount of protein was normalized against the amount of the housekeeper control in each sample.

Generation of reporter cell line for targeted RNA editing assay

In order to generate the reporter cell line for RNA editing, HEK293T cells were seeded in 24-well plates (~150,000 cells per well) to have a confluency of 70-90 % the following day. After 24 h, cells were transfected with 2 µg of the mCherry-T2A-eGFP W58X reporter plasmid (a kind gift of Dr. Joshua Rosenthal, University of Chicago, (Montiel-González et al. 2016)) using Lipofectamine 2000 (ThermoFisher, Cat# 11668019). Then, 48 h after transfections, cells were diluted to single cells in 96-well plates and selected using puromycin (1.5 µg/ml) for two weeks. Clonality was validated by visual inspection with a microscope, and the clones were then screened for the presence of mCherry and absence of eGFP via flow cytometry analysis. The original mCherry-T2A-eGFP W58X was modified by inserting a puromycin resistance cassette within the BglII restriction site to allow selection.

In vitro transcription (IVT) of guide RNAs (gRNAs)

pENTER-U6 coding an optimized RESTORE gRNA[51] to target the eGFP W58X was used to prepare IVT template for gRNAs production. IVT template was generated by PCR using the following primers: forward (5'-AAGCTAATACGACTCACTATAGGTGAATAGTATAACAATATGC-3') and reverse (5'-AAACTACCTGTTCCATGG-3') primers. The forward primer contains the T7 promoter needed for the following IVT reaction. Q5 High-Fidelity DNA Polymerase (New England Biolabs, Cat# M0491) was used for amplification. The PCR product was then purified with the Nucleospin Gel and PCR cleanup kit (Macherey Nagel, Cat# 740609.50) and eluted in 25 µl DEPC-treated water. IVT was performed using the Takara IVTpro T7 mRNA Synthesis Kit (Cat#6144) according to manufacturer's instructions in 20 µl reaction

containing 2 µl of 10X Transfection Buffer, 2 µl of 10x Enzyme mix, 2 µl of 100 mM ATP/UTP/CTP/GTP, 2 µl of 100 mM N6-Methyl-ATP (Jena Bioscience, Cat#NU-1101) in place of ATP, and 1 pmol of DNA template. In vitro transcription reaction was incubated at 37°C for 16 h. DNA template was removed by adding RNAse-free DNAse I (2000 Ul/mL; New England Biolabs, Cat# M0303) for 15 min at 37°C. DNA Dephosphorylation was performed by incubating the IVT product with 2 µl of QuickCip (5000 Ul/mL; New England Biolabs, Cat# M0525) at 37°C for 2 h. IVT gRNAs were purified from the solution by Monarch Clean UP RNA Kit (50 µg) (New England Biolabs, Cat# T2040), eluted in 100 µl DEPC-treated water, and quantified with nanodrop.

Targeted RNA editing assay

HEK293T mCherry-T2A-eGFP W58X cells were seeded in 24-well plates (~150,000 cells per well) to have a confluency of 70-90% the following day. 16 h prior to transfection, the HEK293T mCherry-T2A-eGFP W58X cells were treated with 500 U/mL INFα to induce ADAR1 expression. The cells were then transfected with 20 pmol of gRNA, with and without m6A, using Lipofectamine 2000 (Thermo Fisher Scientific, Cat# 11668019). Flow cytometry analysis for eGFP+ cells was performed at 24h, 48h, 72h post-transfection (FACS Canto II at DKFZ Core Facility Flow Cytometry).

Ribosome profiling (Ribo-Seq)

One day before the experiment, RAW macrophages were seeded at a density of 2×10^6 or 3×10^6 cells per 10 cm dish for WT or METTL3-KO cells, respectively. At different timepoints after addition of 100 ng/ml LPS (Sigma, catalog no. L2630) + 20 ng/ml IFN-γ (PeproTech, catalog no. 315-05), cells were washed in ice-cold PBS supplemented with 100 µg/ml cycloheximide (Roth, Cat# 8682.3), and harvested by scraping in polysome lysis buffer (20 mM Tris-HCl buffer pH 7.4, 10 mM MgCl2, 200 mM KCl, 1 % NP-40, 100 µg/ml cycloheximide, 2 mM DTT, 1 tablet EDTA-free Roche cOmplete Mini Protease Inhibitor per 10 ml). Lysates were rotated for 10 min and then centrifuged at 9,300g for 10 min at 4 °C. About 10% of the lysates were saved as input control. The remaining lysates were digested with RNase I (60 U per A260; Ambion, Cat# AM2294) for 20 min at 4 °C and followed 17.5–50 % sucrose density gradient centrifugation for 1 h 45 min at 40,000 rpm at 4 °C. The monosomal fractions were collected from the gradients into urea buffer (10 mM Tris-HCl pH 7.5, 350 mM NaCl, 10 mM EDTA, 1 % SDS, 7 M urea). RNA was purified by phenol extraction and precipitation in 50% isopropanol by using phenol: chloroform: isoamyl alcohol (AppliChem, Cat# A0944) and GlycoBlue (Ambion, Cat# AM9515). rRNA was then depleted using the Human-Mouse-Rat riboPOOL Kit (siTOOLs, Cat# dp-K096-53). Input RNA was fragmented randomly by alkaline hydrolysis at pH 10.0 for 12 min at 95 °C. Both fragmented input (IN) and ribosome footprints (FP) were isolated by size-selection (25–35 nt) and extraction from a 15 % polyacrylamide Tris-borate-EDTA-urea gel. Purified RNAs were

phosphorylated at their 5' end with 10 U T4 PNK (NEB, Cat# M0201S), 40 U RNase OUT (Invitrogen, Cat# 10777019) and 1 mM ATP in T4 PNK reaction buffer for 1.5 h at 37 °C.

After end-repair, libraries were generated with the NEBNext Multiplex Small RNA Library Prep Kit (NEB, Cat# E7300) according to the manufacturer's manual. To determine the required number of PCR cycles, 1 µl of cDNA per sample was diluted 8 times and used for a qPCR reaction (forward primer: 5'-GTTCAGAGTTCTACAGTCCGA-3', reverse primer: 5'-CCTTGGCACCCGAGAATTCCA-3') using SybrGreen master mix (Applied Biosystems, Cat# A25742) on a QuantStudio Real-Time PCR System. The highest threshold cycle determined among all samples was used for library preparation. The resulting libraries were purified by 10% polyacrylamide Tris-borate-EDTA gels following the manufacturer's instructions and sequenced on a NextSeq550 device (Illumina) with SE75 mode, acquiring an average 8 million reads per sample.

Bioinformatic analysis of Ribo-Seq data

Sequences were demultiplexed and converted to fastq files using bcl2fastq v.2.20. Adapters were removed with the FASTX-toolkit v.0.0.13, retaining only sequences at least 28 nt long. The four random nucleotides at the beginning and the end of the reads were trimmed with an in-house-developed Perl script. The trimmed reads were mapped to tRNA and rRNA sequences (as downloaded from the UCSC Genome Browser) by bowtie v0.12.8, allowing a maximum of two mismatches and reporting all alignments in the best stratum (settings: -a --best --stratum -v 2). Reads that did not map to tRNA or rRNA sequences were aligned to the mouse transcriptome (Gencode VM18 as downloaded from the UCSC Genome Browser wgEncodeGencodeBasicVM18 table). Only reads between 25 and 35 nt long, and mapping to ORFs of isoforms arising from one specific gene (as defined by a common gene symbol) were counted. An offset of 12 nt upstream of the start codon and 15 nt upstream of the stop codon with respect to the 5' end of the read was assumed. Translation efficiencies for each condition were calculated and compared between METTL3-KO and control cells using DESeq2[52] . The downstream analysis included only those genes for which DESeq2 could calculate adjusted P values (Wald test, Benjamini–Hochberg adjustment) for the fold change in translation efficiency. Data can be found in SupplFiles-Table-6.

Illumina RNA-seq data processing

Adapters were trimmed using Trimmomatic v0.38[53] with follow command line:

"trimmomatic.sh PE -threads 15 /${S_name}_R1.fastq.gz /${S_name}_R2.fastq.gz /Trimmed/${S_name}_R1_paired.fastq.gz /Trimmed/${S_name}_R1_unpaired.fastq.gz

/Trimmed/${S_name}_R2_paired.fastq.gz /Trimmed/${S_name}_R2_unpaired.fastq.gz ILLUMINACLIP:/Illumina.fa:3:30:7 MINLEN:50”

Alignment of fastq files to the UCSC mm10 genome was performed using STAR 2 v.2.5.3.a[54] and the parameters detailed below.

“STAR --runMode alignReads --readFilesCommand zcat --genomeDir /UCSC_GRCm38/STAR_index_2.5.3a --readFilesIn ${S_name}R1_paired.fastq.gz ${S_name}_R2_paired.fastq.gz --outFileNamePrefix ${S_name} --runThreadN 10 --outFilterMultimapNmax 1 --outSAMstrandField intronMotif --outSAMtype BAM SortedByCoordinate”.
Bams quality was checked using qualimap v2.2[55]. Output bam files were sorted and indexed using samtools v1.5[56].

Illumina RNA-editing calling and processing

RNA editing candidates were identified using REDItools v2.0[57], employing the reditools.py script with the following parameters:

“reditools.py -f ${S_name}_Aligned.sortedByCoord.out.sorted.dedup.bam -o /REDITOOLED/${S_name}_Aligned.sorted_reditooled.txt -s 2 -T 2 -os 4 -m /REDITOOLED/homopol/${S_name}_Aligned.sorted_homopol.txt -c /REDITOOLED/homopol/${S_name}_Aligned.sorted_homopol.txt -r /UCSC_GRCm38/mm10.fa -sf /UCSC_GRCm38/Splicesites/mm10_splicesites.ss -q 25 -bq 35 -mbp 10 -Mbp 10”

Key parameter settings included a minimum read mapping quality of 25 (-q 25), a minimum base quality of 35 (-bq 35), and exclusion of the first and last 10 bases of each read (-mbp 10 -Mbp 10). Additional parameters specified were: strand-specific mode 2 (-s 2), strand confidence mode 2 (-T 2), and a minimum homopolymer length of 4 (-os 4).

The output files generated by Reditool were processed using a custom in-house script (1.Make_reditoolbackground.R). This script is designed to identify genomic regions that consistently exhibit no edits in the context of A-to-G transitions, representing A-to-I editing as detected by Illumina sequencing (Ctrl_Positions). The script executes the following steps:

Filtering: ADAR-KO Reditool output files are processed to discard sites with more than one substitution type. Only genomic positions with a minimum coverage of 10 reads and no substitutions reported (indicated by the AllSubs column = "-") are retained.
Replicate and Sample Type Selection: Genomic positions are required to be present in at least 2 out of 3 biological replicates and in at least 2 out of 4 sample conditions, ensuring a consistency threshold of 50%.

Aggregation: The script aggregates genomic positions by genomic region and sample type. For each site, the median values of read coverage and the frequency of the alternative allele (expected to approximate 0) are calculated.

These steps are designed to ensure the reliability and consistency of RNA editing calls across the studied samples, enhancing subsequent filtering of false positives and SNPs.

In the next step, the in-house script “2.0.0.RNA_editing_Filtering.R” utilizes the previously generated list of genomic positions (Ctrl_Positions) to identify overlapping sites in CTRL and METTL3-KO samples that exhibit A-to-G mutations, indicative of A-to-I editing as detected by Illumina sequencing. The filtering criteria for retaining candidate editing events involve two main stages:

1. Raw Editing Sites Database Creation.
This step aims at reducing the file size and optimizing subsequent steps for faster processing. The criteria applied during this stage are as follows:
Filtering Covered Positions: Genomic positions (Ctrl_Positions) are filtered to keep only those with a median coverage of ≥10 across sample replicates.
Ctrl Positions Matching: Positions are cross-referenced with the previous filtered Ctrl_Positions, and only matching sites are retained.
Filtering Editing Candidates: Genomic positions with multiple substitution types are discarded, while positions exhibiting A-to-G substitutions and a coverage of ≥5 are retained.

2. Refining Candidate Edited Positions.
Replicate and Sample Group Consistency: Candidate edited positions must be present in at least 2 out of 3 biological replicates and in at least 2 out of 8 sample group conditions.
Coverage: Candidate edited positions with a median coverage of ≥10 within sample replicates are kept.
Editing Frequency Support: Candidate edited positions are further filtered based on the median count of read supporting the editing site of ≥5 across sample replicates.

The script produces three output files, each tailored for specific analyses in this study:

2.Editing_sites_db_Gt10_Al5_Mc10.txt.gz: This file contains a list of edited sites filtered according to the criteria outlined above. It will be referred to as DB1 in this study.

2.Editing_complete_db_Gt10_Al5_Mc5.rds: This database includes a comprehensive list of genomic positions with editing observed in some samples (DB1). It highlights the presence of unedited positions overlapping with edited sites. This file is used for analyses requiring all positions, such as differential editing analysis, and will be referred to as DB2 in this study.

2.Editing_baseline_db_Gt10.rds: This file contains editing candidates with a coverage of ≥5. It is particularly useful for adjusting other filtering criteria, such as estimating consistency across sample groups or calculating global editing site counts and editing frequencies. This file will be referred to as DB3 in this study.

3. Editing sites per sample quantification.

The number of mapped bases for each sample was obtained using Samtools stats. This value was then used to normalize the corresponding number of editing sites per sample. The normalization formula applied is as follows:

$$Normalized\ Editing\ Sites = \frac{Number\ of\ Editing\ Sites}{\frac{Mapped\ Bases}{10^6}}$$

This normalization ensures that the number of editing sites is scaled relative to sequencing depth, enabling more reliable comparisons between samples.

DB3 was used to count the number of editing sites, applying the following filtering criteria: editing sites present in at least 2 out of 3 biological replicates, a median total coverage of ≥10, and a median number of reads supporting editing sites of ≥5. All positions with an editing frequency ≠ 0 were then included in the count.

This filtering approach undoubtedly increases the potential inclusion of low-quality editing sites or false positives. However, assuming the error rate remains consistent across all samples, any observed differences between samples should primarily reflect true differences in editing sites, even if of lower quality.

4. Differentially Edited sites detection

Differential editing sites (DES) were identified using the DSS[58–60] R package, implemented in an in-house script “7.0.Differential_RNA_Editing_DSS.R” with the smoothing option disabled. Originally developed for differential methylation (DM) detection, DSS employs a rigorous Wald test for beta-binomial distributions. The test statistics account for both biological variations (characterized by the dispersion parameter) and sequencing depth. Candidate editing sites from DB2 were used as input for this analysis. The log2 fold change (log2FC) was calculated using the following formula:

$$Log2FC = log2(\mu_1) - log2(\mu_2)$$

Gene expression analysis

The quantification was performed using Salmon v0.14.2[61] in mapping-based mode, providing an efficient and accurate method for transcript quantification. The following command line was used to execute Salmon:

“salmon quant --numBootstraps 20 -i /UCSC_GRCm38/SALMON_index/ -l A -1 /Trimmed/${Sample_name}_R1_paired.fastq.gz -2 /Trimmed/${Sample_name}_R2_paired.fastq.gz -p 25 -o /SALMON_expr/${Sample_name} --validateMappings”

The Salmon outputs were imported into EdgeR[62] via the tximport[63] package, which produces gene-level estimated counts and an associated edgeR offset matrix. Differential analysis for gene counts was performed using the EdgeR[62], implemented in an in-house code. Significantly upregulated/downregulated genes were determined by abs(logFC)>0.5 and FDR < 0.05. The volcano plot was generated using the EnhancedVolcano R package[64].

Nanopore direct-RNAseq pre-processing

The pod5 files were basecalled using the ONT basecaller Dorado v0.7.0, with the models “rna004_130bps_hac@v5.0.0” and “rna004_130bps_hac@v5.0.0_m6A@v1” for the kit “SQK-RNA004”. Basecalling was performed on a GPU (Tesla V100-SXM2-32GB).
The command line used is as follows:

“dorado basecaller --min-qscore 6 --emit-moves hac,m6A /ont/raw/i0039410/data/1184237/pod5_pass/ --reference /UCSC_GRCm38/mm10.fa --mm2-preset splice:uf:k14 > /ONT/Bams_dorado_Genome/File.bam”

--hac,m6A: Specifies the models used for basecalling. The hac model (rna004_130bps_hac@v5.0.0) is the high-accuracy model for standard basecalling, while the m6A model

(rna004_130bps_hac@v5.0.0_m6A@v1) is used for detecting m6A RNA modifications. At the time of our analysis, the detection of inosine modifications was not available as an option in the modification detection settings.

--mm2-preset splice:uf:k14: Configures the minimap2 alignment preset for mapping RNA reads, optimized for spliced alignment[65].

Output bam files were sorted and indexed using samtools v1.5.

Nanopore m6a detection

The BAM files were processed to generate modification BED files using Modkit v0.3.1. For m6A calling, the parameters --filter-threshold A:0.8 and --mod-threshold m:0.99 were applied, as determined by the modification probability density plot and HeatMap generated using Modkit sample-probs output files (SupplFig. 3A).

Modkit sample-porbs command line:
“modkit sample-probs -t 20 --percentiles 0.1,0.5,0.95 -f 0.3 --hist --only-mapped --force --prefix ${S_name} -o /m6a_Res/${S_name}.bam”

Modkit pileup command line:
“modkit pileup -t 20 --log-filepath /m6a_Res/Pileup/${S_name}.log --sampling-frac 0.4 --max-depth 20000 --with-header --filter-threshold A:0.8 --mod-thresholds a:0.99 ${S_name}.bam /m6a_Res/Pileup/${S_name}.bed”

M6a preprocessing

Modkit sample-probs results revealed no discernible differences in m6A counts between METTL3-KO and control samples when using threshold values below 0.99 (SupplFig. 2F). This finding suggests a high likelihood of false-positive m6A site detection at lower thresholds, or, less plausibly, the presence of residual methylation-mediated by other methyltransferases or potential miscalling of m1A as m6A.

To discover potential m6A sites, we began by identifying differentially methylated (DM) candidates under the assumption that changes in methylation frequency highlight bona fide m6A modifications dependent on METTL3. We then performed two separate comparisons using METTL3-KO (untreated and LPS-IFNγ 24 h) as the negative control. Specifically, we compared:

ADAR (untreated and LPS-IFNγ 24 h) versus METTL3-KO (untreated and LPS-IFNγ 24 h).

CTRL (untreated and LPS 24 h) versus METTL3-KO (untreated and LPS-IFNγ 24 h).

These comparisons allowed us to pinpoint potential DM sites that differ between ADAR or CTRL samples and METTL3-KO under corresponding conditions (SupplFig. 3G). These comparisons employed the R package DSS[58–60] within an in-house script, with the smoothing option disabled. While smoothing is designed for CpG island analyses, where m6A sites often exhibit strong spatial correlations, it can produce false positives in RNA data by labeling m6a site flanking regions as m6A-positive despite zero actual m6a read count.

For the DM analysis, genomic positions were initially filtered as follows:

Coverage Threshold: Only positions with a coverage of ≥10 reads across samples were retained.

Replicate and Sample Group Consistency: Candidate edited positions must be present in at least 2 out of 3 biological replicates, and in both sample groups being compared.

Eliminating positions that showed no change between target and METTL3-KO samples yielded a final set of m6A candidate sites, including their genomic coordinates, coverage data, and log2 fold-change relative to the corresponding knockout samples. At this stage, no filtering was applied based on the number of modified reads supporting a methylated position or logFC; these thresholds will be established later, according to the specific requirements of downstream analyses.

In a second step, the m6A candidate sites identified in the previous comparisons were merged to generate a comprehensive list of potential m6A sites. This list was then used to retrieve corresponding positions from the BED methylation files (for ADAR-KO and CTRL samples), producing a consolidated dataset of potential m6A positions observed in 2 or more samples (SupplFiles-1.2.0.All_m6a_Positions_DMA_LFC05_annotated_DB1.rds - DB1m6a).

Notably, this approach also incorporates unmethylated positions overlapping putative m6A sites. The sites used for list building were filtered using the criteria |Log2FC| ≤ 0.5 and FDR < 0.05, ensuring the selection of m6A sites that were either unmethylated or poorly methylated in METTL3-KO samples. Any additional filtering of these methylated positions was applied based on the specific requirements of subsequent analyses, ensuring data relevance and methodological consistency.

M6a and AtoI Editing sites effect prediction and Annotation

The impact of editing sites was analyzed using the Ensembl Variant Effect Predictor (VEP)[66] and Homer[67], integrated into an in-house R script executed via the command line. M6A sites were annotated and profiled across gene body regions using ChIPseeker[68] and Homer[67]. The list of macrophages, double strand Response, phagocytosis makers downloaded from Mouse Genome Informatics using the following Gene

Ontology terms: GO:0042116 (macrophages activation), GO:0006909 (phagocytosis), GO:0034340 (response to type I interferon), GO:0043331 (response to dsRNA).

M6a sites per sample quantification

For this analysis, m6A (DB1m6a) sites were selected based on criteria requiring a minimum total coverage of 10 reads and at least 5 reads supporting the m6A site. Although total coverage and the number of supporting reads may not always be sufficient to reliably distinguish true m6A sites from false positives, the error rate is expected to be consistent across the entire library of samples. Consequently, any observed changes, if present, should be attributed to genuine m6A sites. The number of m6A sites was then normalized using the same approach previously applied to editing sites.

M6a Motif analysis

m6A sites considered for the analysis were taken from untreated Ctrl samples (DB1m6a). The motif was tested, and identified sites were filtered using the following criteria: median coverage ≥ 10, median m6A frequency ≥ 5, and median minimum number of reads supporting m6A sites ≥ 5, using regular expressions ([AGT][AG]A[C][ACT]) for DRACH motif and ([AGT][AG]A[C][.]) for less strict DRACN motif.

A-to-I - m6a modification interplay

The editing and m6A sites used to study the potential relationship between the two modifications were initially analyzed only in Ctrl-24h. We selected Ctrl-24h post-stimulation because:

-Both enzymatic machinery (METTL3 and ADAR1) are fully functional, ensuring that both modifications can occur.

-Editing frequency peaks at 24 hours, making it the ideal time point to test whether a relationship between m6A and A-to-I editing exists.

-Furthermore, the same editing sites identified in Ctrl-24h were used for direct comparison with the corresponding edited regions in METTL3-KO, allowing us to assess how m6A depletion could affect editing levels.

Based on these assumptions, editing sites for the analysis were selected from DB2 using the following criteria:

Median coverage ≥ 20

Median number of reads supporting editing ≥ 5

Median editing frequency ≥ 0.05

The same filtering cutoffs were applied to m6A (DB1m6a) site selection.

For the final dataset, the distance between each editing site and the closest m6A site was calculated using distanceToNearest, GRanges's function[69]. Furthermore, the number of editing sites and the number of methylated sites per transcript feature were also included and utilized for a more detailed statistical model (Supplementary Material).

Only modification events occurring in the 3' UTR were considered for the analysis. The distance and m6A level ranking, as well as the resulting classification, were set up based on quantiles calculated over both distance and m6A levels to ensure a systematic categorization (Fig. 6H-G).

Data Availability

The data for this study will be made available once the manuscript has been conditionally accepted under BioProject number PRJNA1232413. The code used for this manuscript will be available once the manuscript has been conditionally accepted at Papavasiliou (Github link) and https://github.com/Salvobioinfo .

Acknowledgments

We thank the Next Generation Sequencing Core Facility and the Flow Cytometry Core Facility, German Cancer Research Center (DKFZ), for providing excellent sequencing and sorting services. We gratefully acknowledge funding by the Deutsche Forschungsgemeinschaft (DFG, German Research Foundation) – RTG2727 – 445549683 (to VG), by SVB TRR319-RMaP (to SdG, FNP, VG, CK and GS) and the HI-TRON Kick-Start Seed Funding Program 2021 awarded to RP.

Authors contribution

VG, SdG, FNP and GS conceived the idea of the work. VG created the clonal RAW knockout cell lines and performed all experiments including Nanopore sequencing concerning the RAW cell line with the exception of sample processing and data analysis of Ribosome Sequencing which was performed by CK. IT and SdG performed pre-processing of the Nanopore Sequencing data. SdG performed all other bioinformatic analyses concerning the Illumina and Nanopore Sequencing data. JB and SdG created the regression model and statistics. RP designed and generated with the help of AA the plasmid coding the gRNA targeting eGFP and the reporter cell line. JPL and LP designed and performed experiments using IVT gRNAs containing m6A. VG, SdG, and FNP wrote the manuscript, which was reviewed by RP, GS, CK, JPL, and LP.

References

1. Shi, H., Chai, P., Jia, R. & Fan, X. Novel insight into the regulatory roles of diverse RNA modifications: Re-defining the bridge between transcription and translation. *Mol. Cancer* **19**, 78 (2020).
2. Meyer, K. D. *et al.* Comprehensive Analysis of mRNA Methylation Reveals Enrichment in 3′ UTRs and near Stop Codons. *Cell* **149**, 1635–1646 (2012).
3. Dominissini, D. *et al.* Topology of the human and mouse m6A RNA methylomes revealed by m6A-seq. *Nature* **485**, 201–206 (2012).
4. Liu, J. *et al.* A METTL3–METTL14 complex mediates mammalian nuclear RNA N6-adenosine methylation. *Nat. Chem. Biol.* **10**, 93–95 (2014).
5. Ke, S. *et al.* A majority of m6A residues are in the last exons, allowing the potential for 3’ UTR regulation. *Genes Dev.* **29**, 2037–2053 (2015).
6. Zheng, G. *et al.* ALKBH5 is a mammalian RNA demethylase that impacts RNA metabolism and mouse fertility. *Mol. Cell* **49**, 18–29 (2013).
7. Jia, G. *et al.* N6-Methyladenosine in nuclear RNA is a major substrate of the obesity-associated FTO. *Nat. Chem. Biol.* **7**, 885–887 (2011).
8. Wang, X. *et al.* N6-methyladenosine Modulates Messenger RNA Translation Efficiency. *Cell* **161**, 1388–1399 (2015).
9. Wang, X. *et al.* N6-methyladenosine-dependent regulation of messenger RNA stability. *Nature* **505**, 117–120 (2014).
10. Meyer, K. D. *et al.* 5′ UTR m6A Promotes Cap-Independent Translation. *Cell* **163**, 999–1010 (2015).
11. Zhou, J. *et al.* Dynamic m6A mRNA methylation directs translational control of heat shock response. *Nature* **526**, 591–594 (2015).
12. Xiao, W. *et al.* Nuclear m(6)A Reader YTHDC1 Regulates mRNA Splicing. *Mol. Cell* **61**, 507–519

(2016).

13. Huang, H. *et al.* Recognition of RNA N6-methyladenosine by IGF2BP Proteins Enhances mRNA Stability and Translation. *Nat. Cell Biol.* **20**, 285–295 (2018).
14. Wang, H., Tang, A., Cui, Y., Gong, H. & Li, H. LRPPRC facilitates tumor progression and immune evasion through upregulation of m6A modification of PD-L1 mRNA in hepatocellular carcinoma. *Front. Immunol.* **14**, 1144774 (2023).
15. Alarcón, C. R. *et al.* HNRNPA2B1 is a mediator of m6A-dependent nuclear RNA processing events. *Cell* **162**, 1299–1308 (2015).
16. Roundtree, I. A. *et al.* YTHDC1 mediates nuclear export of N6-methyladenosine methylated mRNAs. *eLife* **6**, e31311 (2017).
17. Gao, Y. *et al.* m6A Modification Prevents Formation of Endogenous Double-Stranded RNAs and Deleterious Innate Immune Responses during Hematopoietic Development. *Immunity* **52**, 1007-1021.e8 (2020).
18. Qiu, W. *et al.* N6-methyladenosine RNA modification suppresses antiviral innate sensing pathways via reshaping double-stranded RNA. *Nat. Commun.* **12**, 1582 (2021).
19. Bass, B. L. RNA Editing by Adenosine Deaminases That Act on RNA. *Annu. Rev. Biochem.* **71**, 817–846 (2002).
20. Wulff, B.-E. & Nishikura, K. Substitutional A-to-I RNA editing. *Wiley Interdiscip. Rev. RNA* **1**, 90–101 (2010).
21. Mannion, N. M. *et al.* The RNA-Editing Enzyme ADAR1 Controls Innate Immune Responses to RNA. *Cell Rep.* **9**, 1482–1494 (2014).
22. Pestal, K. *et al.* Isoforms of RNA-Editing Enzyme ADAR1 Independently Control Nucleic Acid Sensor MDA5-Driven Autoimmunity and Multi-organ Development. *Immunity* **43**, 933–944 (2015).
23. Li, Y. *et al.* RNA Editing Enzyme ADAR1 Regulates METTL3 in an Editing Dependent Manner to

Promote Breast Cancer Progression via METTL3/ARHGAP5/YTHDF1 Axis. *Int. J. Mol. Sci.* **23**, 9656 (2022).

24. Tassinari, V. *et al.* ADAR1 is a new target of METTL3 and plays a pro-oncogenic role in glioblastoma by an editing-independent mechanism. *Genome Biol.* **22**, 51 (2021).
25. Xiang, J.-F. *et al.* N6-Methyladenosines Modulate A-to-I RNA Editing. *Mol. Cell* **69**, 126-135.e6 (2018).
26. Liu, Y. *et al.* The N6-methyladenosine (m6A)-forming enzyme METTL3 facilitates M1 macrophage polarization through the methylation of STAT1 mRNA. *Am. J. Physiol.-Cell Physiol.* **317**, C762–C775 (2019).
27. Wang, J., Yan, S., Lu, H., Wang, S. & Xu, D. METTL3 Attenuates LPS-Induced Inflammatory Response in Macrophages via NF-κB Signaling Pathway. *Mediators Inflamm.* **2019**, 3120391 (2019).
28. Zong, X. *et al.* Mettl3 Deficiency Sustains Long-Chain Fatty Acid Absorption through Suppressing Traf6-Dependent Inflammation Response. *J. Immunol. Author Choice* **202**, 567–578 (2019).
29. Cai, D., Sun, C., Murashita, T., Que, X. & Chen, S.-Y. ADAR1 non-editing function in macrophage activation and abdominal aortic aneurysm. *Circ. Res.* **132**, e78–e93 (2023).
30. Sun, C., Cai, D. & Chen, S.-Y. ADAR1 promotes systemic sclerosis via modulating classic macrophage activation. *Front. Immunol.* **13**, 1051254 (2022).
31. Schott, J. *et al.* Translational Regulation of Specific mRNAs Controls Feedback Inhibition and Survival during Macrophage Activation. *PLOS Genet.* **10**, e1004368 (2014).
32. Wang, X. *et al.* The m6A Reader IGF2BP2 Regulates Macrophage Phenotypic Activation and Inflammatory Diseases by Stabilizing TSC1 and PPARγ. *Adv. Sci.* **8**, 2100209 (2021).
33. Akira, S., Takeda, K. & Kaisho, T. Toll-like receptors: critical proteins linking innate and acquired immunity. *Nat. Immunol.* **2**, 675–680 (2001).
34. Pecori, R. *et al.* ADAR1-mediated RNA editing promotes B cell lymphomagenesis. *iScience* **26**, 106864 (2023).

35. Liddicoat, B. J. *et al.* RNA editing by ADAR1 prevents MDA5 sensing of endogenous dsRNA as nonself. *Science* **349**, 1115–1120 (2015).

36. Guerriero, J. L. Chapter Three - Macrophages: Their Untold Story in T Cell Activation and Function. in *International Review of Cell and Molecular Biology* (eds. Galluzzi, L. & Rudqvist, N.-P.) vol. 342 73–93 (Academic Press, 2019).

37. Vukić, D. *et al.* Distinct interactomes of ADAR1 nuclear and cytoplasmic protein isoforms and their responses to interferon induction. *Nucleic Acids Res.* **52**, 14184–14204 (2024).

38. Montiel-González, M. F., Vallecillo-Viejo, I. C. & Rosenthal, J. J. C. An efficient system for selectively altering genetic information within mRNAs. *Nucleic Acids Res.* **44**, e157 (2016).

39. Monian, P. *et al.* Endogenous ADAR-mediated RNA editing in non-human primates using stereopure chemically modified oligonucleotides. *Nat. Biotechnol.* **40**, 1093–1102 (2022).

40. Medzhitov, R. & Horng, T. Transcriptional control of the inflammatory response. *Nat. Rev. Immunol.* **9**, 692–703 (2009).

41. Hargreaves, D. C., Horng, T. & Medzhitov, R. Control of Inducible Gene Expression by Signal-Dependent Transcriptional Elongation. *Cell* **138**, 129–145 (2009).

42. Mosser, D. M. & Edwards, J. P. Exploring the full spectrum of macrophage activation. *Nat. Rev. Immunol.* **8**, 958–969 (2008).

43. Zaccara, S. & Jaffrey, S. R. A Unified Model for the Function of YTHDF Proteins in Regulating m6A-Modified mRNA. *Cell* **181**, 1582-1595.e18 (2020).

44. Azulay, G. *et al.* A dual-function phage regulator controls the response of cohabiting phage elements via regulation of the bacterial SOS response. *Cell Rep.* **39**, (2022).

45. Véliz, E. A., Easterwood, L. M. & Beal, P. A. Substrate Analogues for an RNA-Editing Adenosine Deaminase: Mechanistic Investigation and Inhibitor Design. *J. Am. Chem. Soc.* **125**, 10867–10876 (2003).

46. Nishikura, K. Functions and Regulation of RNA Editing by ADAR Deaminases. (2010) doi:10.1146/annurev-biochem-060208-105251.

47. Jones, A. N., Tikhaia, E., Mourão, A. & Sattler, M. Structural effects of m6A modification of the Xist A-repeat AUCG tetraloop and its recognition by YTHDC1. *Nucleic Acids Res.* **50**, 2350–2362 (2022).

48. Liu, B. *et al.* A potentially abundant junctional RNA motif stabilized by m6A and Mg2+. *Nat. Commun.* **9**, 2761 (2018).

49. Wave Life Sciences Ltd. *A Phase 1, Randomized, Double-Blind, Placebo-Controlled, Safety, Tolerability, and Pharmacokinetic Study of Single Ascending Doses and Multiple Doses of WVE-006 in Healthy Participants*. https://clinicaltrials.gov/study/NCT06186492 (2023).

50. Wave Life Sciences Announces First-Ever Therapeutic RNA Editing in Humans Achieved in RestorAATion-2 Trial of WVE-006 in Alpha-1 Antitrypsin Deficiency - Wave Life Sciences. https://ir.wavelifesciences.com/node/11731.

51. Merkle, T. *et al.* Precise RNA editing by recruiting endogenous ADARs with antisense oligonucleotides. *Nat. Biotechnol.* **37**, 133–138 (2019).

52. Love, M. I., Huber, W. & Anders, S. Moderated estimation of fold change and dispersion for RNA-seq data with DESeq2. *Genome Biol.* **15**, 550 (2014).

53. Bolger, A. M., Lohse, M. & Usadel, B. Trimmomatic: A flexible trimmer for Illumina sequence data. *Bioinformatics* **30**, 2114–2120 (2014).

54. Dobin, A. *et al.* STAR: Ultrafast universal RNA-seq aligner. *Bioinformatics* **29**, 15–21 (2013).

55. Okonechnikov, K., Conesa, A. & García-Alcalde, F. Qualimap 2: Advanced multi-sample quality control for high-throughput sequencing data. *Bioinformatics* **32**, 292–294 (2016).

56. Li, H. *et al.* The Sequence Alignment/Map format and SAMtools. *Bioinformatics* **25**, 2078–2079 (2009).

57. Flati, T. *et al.* HPC-REDItools: a novel HPC-aware tool for improved large scale RNA-editing analysis. *BMC Bioinformatics* **21**, 353 (2020).

58. Wu, H., Wang, C. & Wu, Z. A new shrinkage estimator for dispersion improves differential expression detection in RNA-seq data. *Biostatistics* **14**, 232–243 (2013).

59. Park, Y. & Wu, H. Differential methylation analysis for BS-seq data under general experimental design. *Bioinformatics* **32**, 1446–1453 (2016).

60. Feng, H., Conneely, K. N. & Wu, H. A Bayesian hierarchical model to detect differentially methylated loci from single nucleotide resolution sequencing data. *Nucleic Acids Res.* **42**, e69 (2014).

61. Patro, R., Duggal, G., Love, M. I., Irizarry, R. A. & Kingsford, C. Salmon provides fast and bias-aware quantification of transcript expression. *Nat. Methods* **14**, 417–419 (2017).

62. Robinson, M. D., McCarthy, D. J. & Smyth, G. K. edgeR: a Bioconductor package for differential expression analysis of digital gene expression data. *Bioinforma. Oxf. Engl.* **26**, 139–40 (2010).

63. Soneson, C., Love, M. I. & Robinson, M. D. Differential analyses for RNA-seq: transcript-level estimates improve gene-level inferences. Preprint at https://doi.org/10.12688/f1000research.7563.1 (2016).

64. Lewis M., B. K., Rana S. EnhancedVolcano: Publication-ready volcano plots with enhanced colouring and labeling. (2024).

65. Li, H. Minimap2: pairwise alignment for nucleotide sequences. *Bioinformatics* **34**, 3094–3100 (2018).

66. McLaren, W. *et al.* The Ensembl Variant Effect Predictor. *Genome Biol.* **17**, 122 (2016).

67. Zhang, F. & Chen, J. Y. HOMER: a human organ-specific molecular electronic repository. *BMC Bioinformatics* **12**, S4 (2011).

68. Yu, G., Wang, L.-G. & He, Q.-Y. ChIPseeker: an R/Bioconductor package for ChIP peak annotation, comparison and visualization. *Bioinforma. Oxf. Engl.* **31**, 2382–2383 (2015).

69. Lawrence, M. *et al.* Software for Computing and Annotating Genomic Ranges. *PLOS Comput. Biol.* **9**, e1003118 (2013).

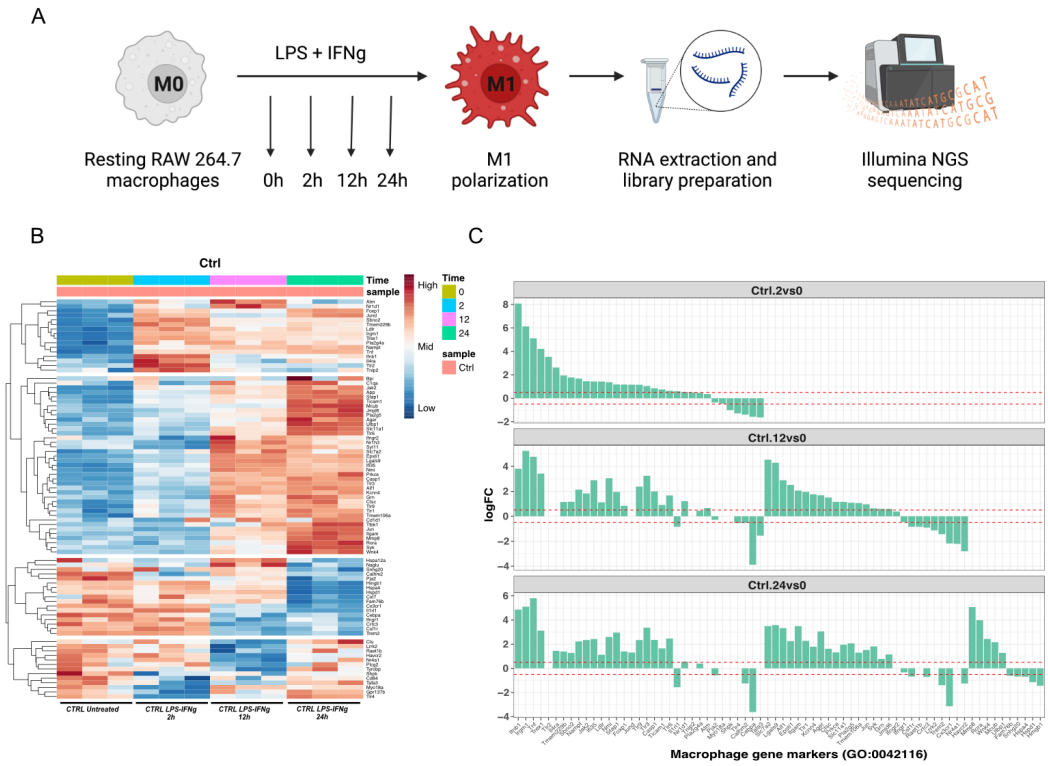

Figure 1. Macrophage response to proinflammatory stimulation. (A) Schematic representation of polarization assay. **(B)** Heatmap of macrophage marker gene expression (GO:0042116). The heatmap illustrates the expression dynamics of macrophage marker genes during LPS-IFNγ treatment over a time course of control samples. Expression values are presented as LogCPM, with rows representing individual genes and columns representing sample replicates at different time points. Hierarchical clustering of genes was performed using Euclidean distance of gene expression profiles, and the resulting dendrogram is displayed on the left. **(C)** LogFC of significantly differentially expressed macrophage marker genes. Genes were selected based on statistical significance (FDR < 0.05).The bar plot displays log2FC values, arranged in descending order of magnitude (left to right), with gene identifiers shown on the x-axis. The increasing time upon treatment is represented from top to bottom. The dotted lines indicate |logFC| = 0.5, representing the threshold for differential expression.

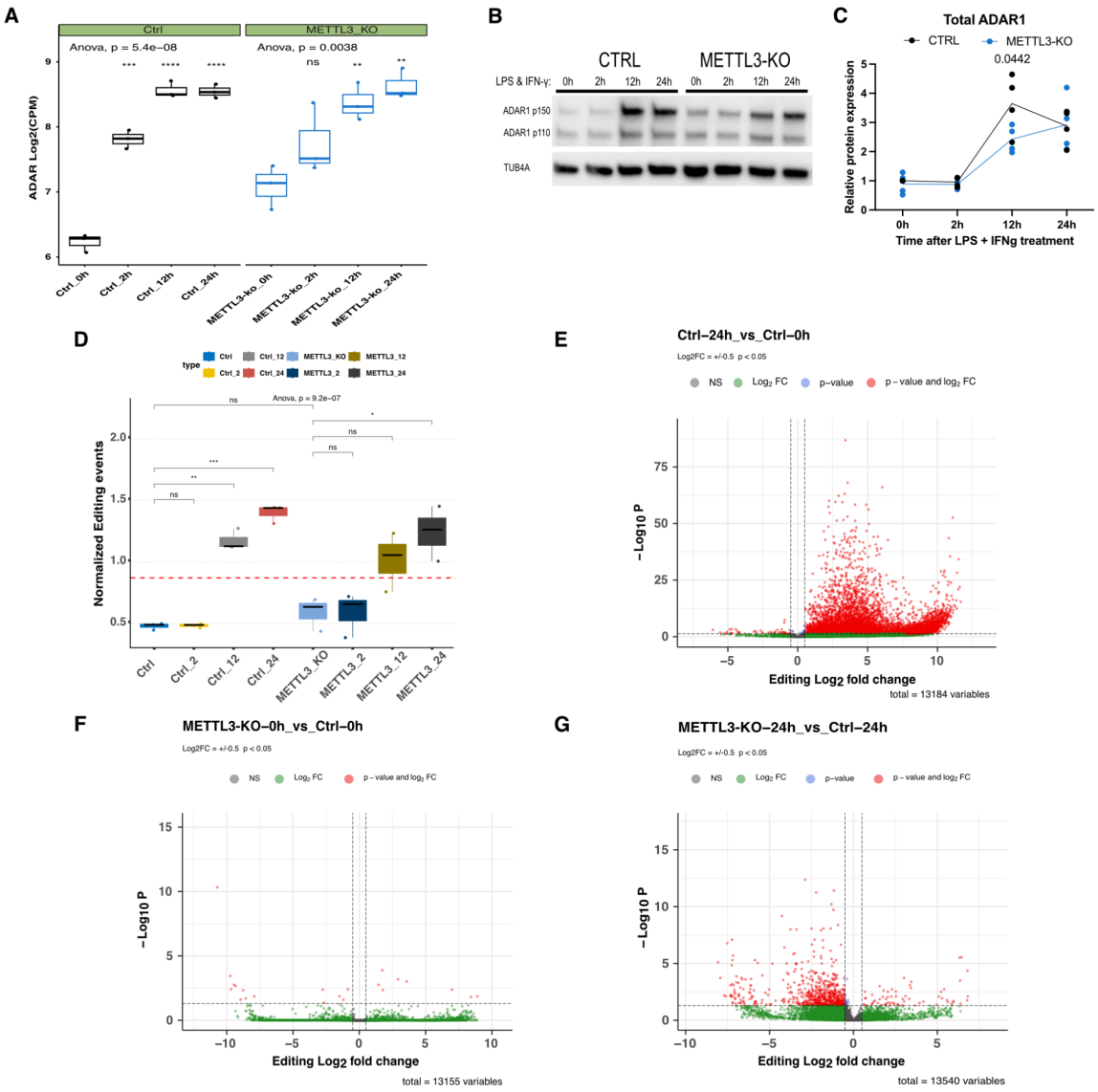

Figure 2. Impact of METTL3 on A-to-I editing during stimulation (A) Boxplots illustrating the expression levels of Adar mRNA across various LPS-IFNγ treatment time points (0, 2, 12, and 24 hours) in Control (Ctrl) and METTL3 Knockout (KO) conditions. **(B)** Representative Western blot of ADAR1 protein expression during the time course of stimulation. **(C)** Quantification of total ADAR1 protein levels. **(D)** Boxplots representing the number of editing events normalized by millions of mapped bases. **(E)** Volcano plot showing differential editing sites in Control (Ctrl) samples after 24 hours of LPS-IFNγ treatment, compared to untreated Ctrl samples. **(F)** Volcano plot showing differential editing sites in untreated METTL3-KO, compared to untreated Ctrl. **(G)** Volcano plot showing differential editing sites in METTL3-KO compared to Ctrl after 24 hours of LPS-IFNγ treatment. In panels **(E–G)**, vertical dashed lines represent log2FC thresholds of -0.5 and 0.5, while horizontal dashed lines indicate a p-value threshold of 0.05. Boxplot **(A-D)** statistical analysis was performed using a global ANOVA test, with pairwise comparisons conducted through post hoc t-tests. Significance levels are denoted as follows: $*p < 0.05$; $**p < 0.01$; $***p < 0.001$; $****p < 0.0001$.

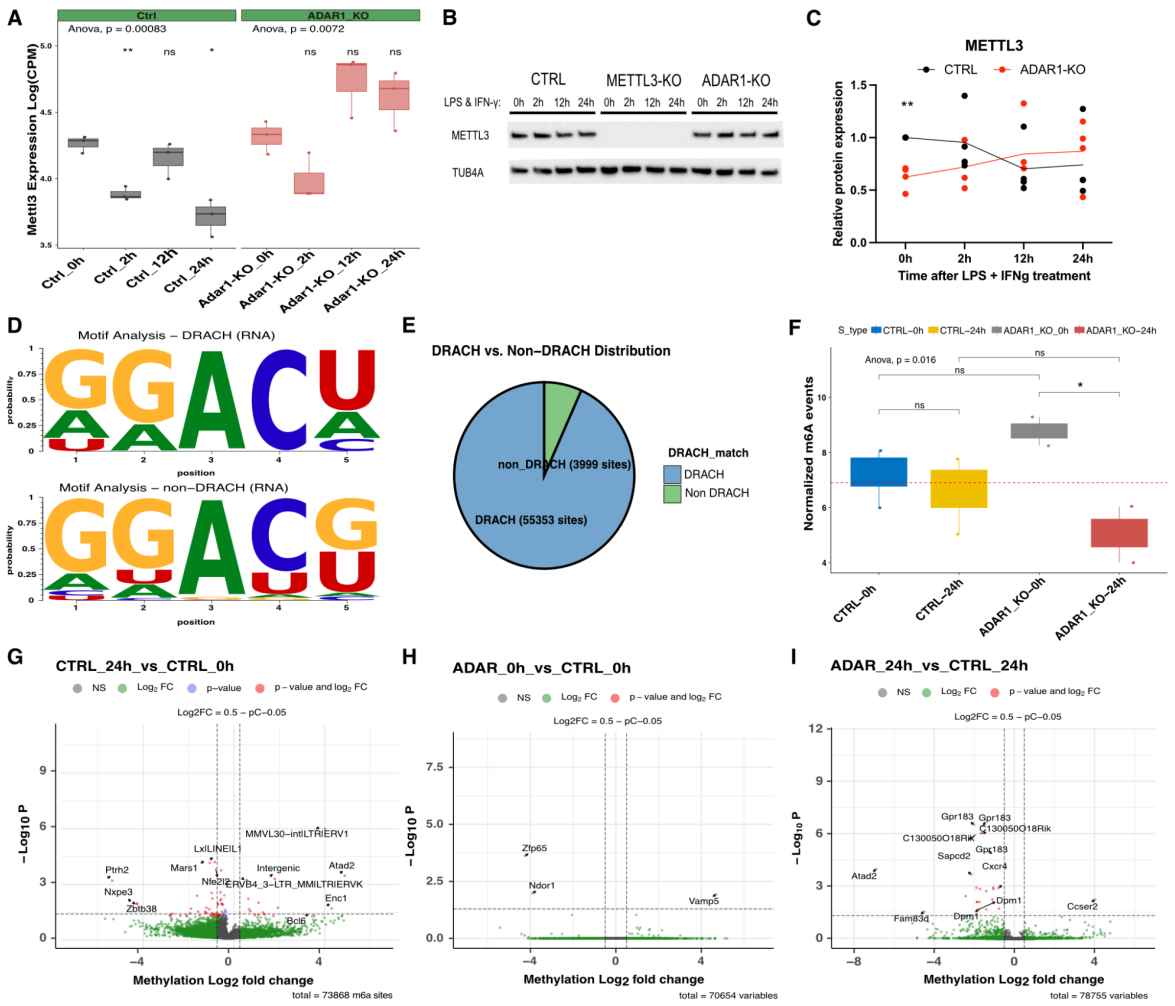

Figure 3. Impact of loss of ADAR1 on m6A levels during stimulation (A) Boxplots illustrating the expression levels of METTL3 mRNA across various LPS-IFNγ treatment time points (0, 2, 12, and 24 hours) in Control (Ctrl) and ADAR Knockout (KO) conditions. (**B)** Representative Western blot of METTL3 protein expression during the time course of stimulation. **(C)** Quantification of METTL3 protein levels. **(D)** Motif analysis of m6A sites obtained from ONT sequencing data, categorized into DRACH and non-DRACH motifs, in m6A sites collected from untreated Ctrl samples. **(E)** Pie chart representing distribution of potential m6A sites located in DRACH vs. non-DRACH motif. **(F)** Boxplots representing the number of m6a events normalized by millions of mapped bases. **(G)** Volcano plot showing differentially methylated sites (DMS) identified in Control (Ctrl) samples after 24 hours of LPS-IFNγ treatment, compared to untreated Ctrl samples. **(H)** Volcano plot showing DMS in untreated ADAR-KO, compared to untreated Ctrl. **(I)** Volcano plot showing DMS in ADAR-KO compared to Ctrl after 24 hours of LPS-IFNγ treatment. In panels **(G–I)**, vertical dashed lines represent log2FC thresholds of -0.5 and 0.5, while horizontal dashed lines indicate a p-value threshold of 0.05. Boxplot **(A-F)** statistical analysis was performed using a global ANOVA test, with pairwise comparisons conducted through post hoc t-tests. Significance levels are denoted as follows: $*p < 0.05$; $**p < 0.01$; $***p < 0.001$; $****p < 0.0001$.

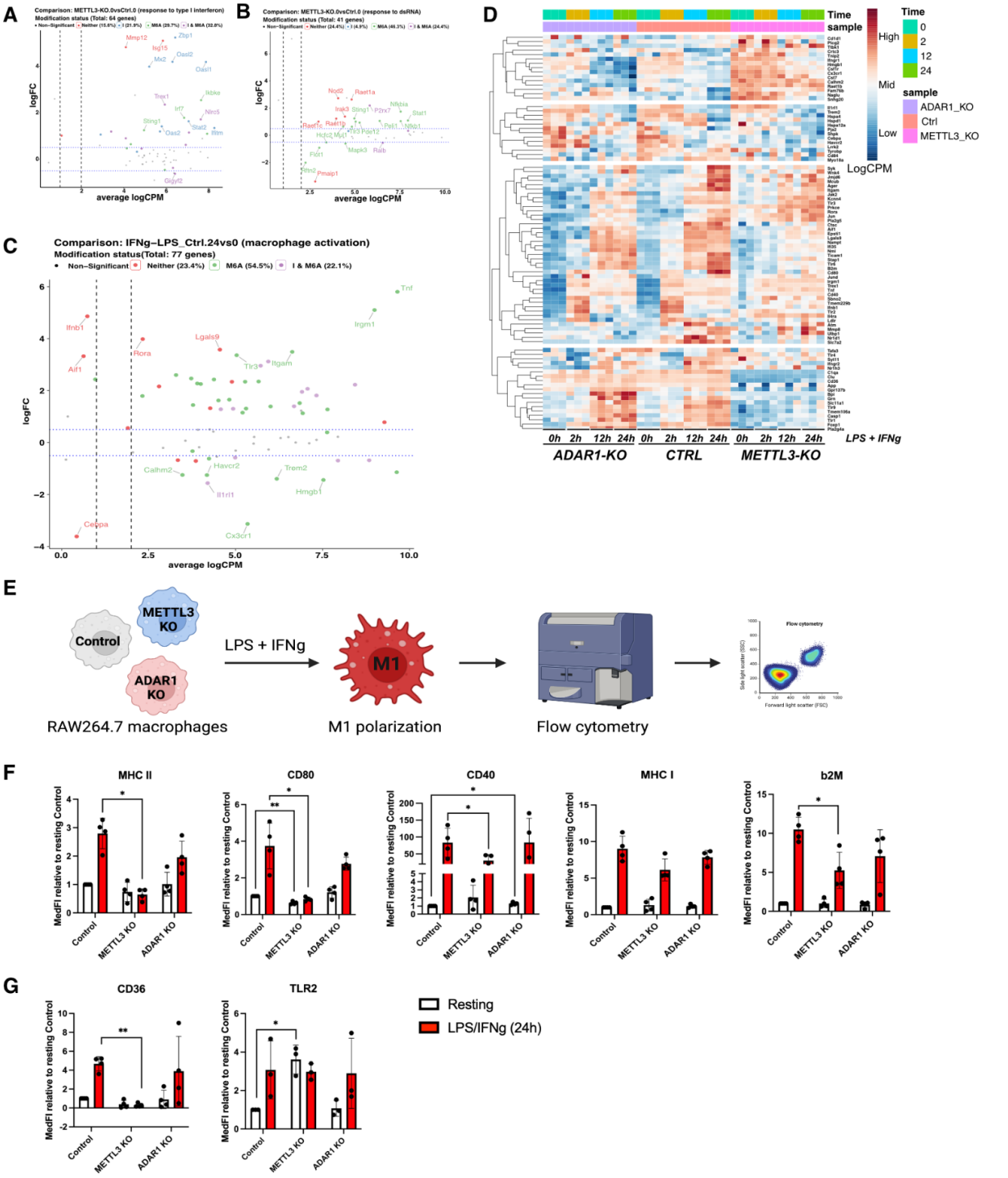
A
Comparison: METTL3-KO.0vsCtrl.0 (response to type I interferon)
Modification status (Total: 64 genes)
Non-Significant
Neither (15.6%)
I (21.9%)
M6A (29.7%)
I & M6A (32.8%)
logFC
average logCPM
B
Comparison: METTL3-KO.0vsCtrl.0 (response to dsRNA)
Modification status (Total: 41 genes)
Non-Significant
Neither (24.4%)
I (4.9%)
M6A (46.3%)
I & M6A (24.4%)
logFC
average logCPM
C
Comparison: IFNg−LPS_Ctrl.24vs0 (macrophage activation)
Modification status(Total: 77 genes)
Non−Significant
Neither (23.4%)
M6A (54.5%)
I & M6A (22.1%)
Tnf
Irgm1
Ifnb1
Lgals9
Rora
Aif1
Tlr3
Itgam
Calhm2
Havcr2
Trem2
Il1rl1
Hmgb1
Cebpa
Cx3cr1
logFC
average logCPM
D
Time
sample
High
Mid
Low
LogCPM
Time
0
2
12
24
sample
ADAR1_KO
Ctrl
METTL3_KO
0h 2h 12h 24h 0h 2h 12h 24h 0h 2h 12h 24h
LPS + IFNg
ADAR1-KO
CTRL
METTL3-KO
E
Control
METTL3 KO
ADAR1 KO
RAW264.7 macrophages
LPS + IFNg
M1
M1 polarization
Flow cytometry
F
MHC II
CD80
CD40
MHC I
b2M
MedFI relative to resting Control
Control
METTL3 KO
ADAR1 KO
G
CD36
TLR2
MedFI relative to resting Control
Control
METTL3 KO
ADAR1 KO
Resting
LPS/IFNg (24h)

Figure 4: Changes in cell surface marker expression in METTL3-KO and ADAR1-KO macrophages. (A-B-D) MA plot showing the mean gene expression (average logCPM) and log fold change (logFC) across all analyzed genes. Each point represents a gene, with the x-axis indicating mean expression and the y-axis representing differential expression between conditions. Color-codes are based on their modification status and differential expression: non-differentially expressed (black), unmodified (red), A-to-I edited (blue), m6A methylated (green), and both edited and methylated (purple). MA plots illustrating differentially expressed genes involved in (**A**) interferon type I signaling (GO:0034340) **(B)** and the dsRNA response (GO:0043331) in METTL3-KO vs. Control (Ctrl) samples without external stimulation. **(C)** MA plot illustrating differentially expressed macrophage activation markers (GO:0042116) in Control (Ctrl) samples at 24 hours post-LPS-IFN-γ treatment, compared with unstimulated Ctrl samples. **(D)** Heatmap showing macrophage marker gene expression across all conditions. Expression values are presented as logCPM, with rows representing individual genes and columns representing sample groups and replicates (three per sample and condition) at different time points after treatment. Hierarchical clustering of genes was performed using Euclidean distance, and the resulting dendrogram is displayed on the left. **(E)** Schematic representation of the workflow. **(F-G)** Flow cytometry analysis of activation-associated cell surface markers at rest and 24h after LPS and IFN-γ treatment. Paired two-tailed t-tests were performed. Significance levels are denoted as: $*p < 0.05$; $**p < 0.01$; $***p < 0.001$; $****p < 0.0001$.

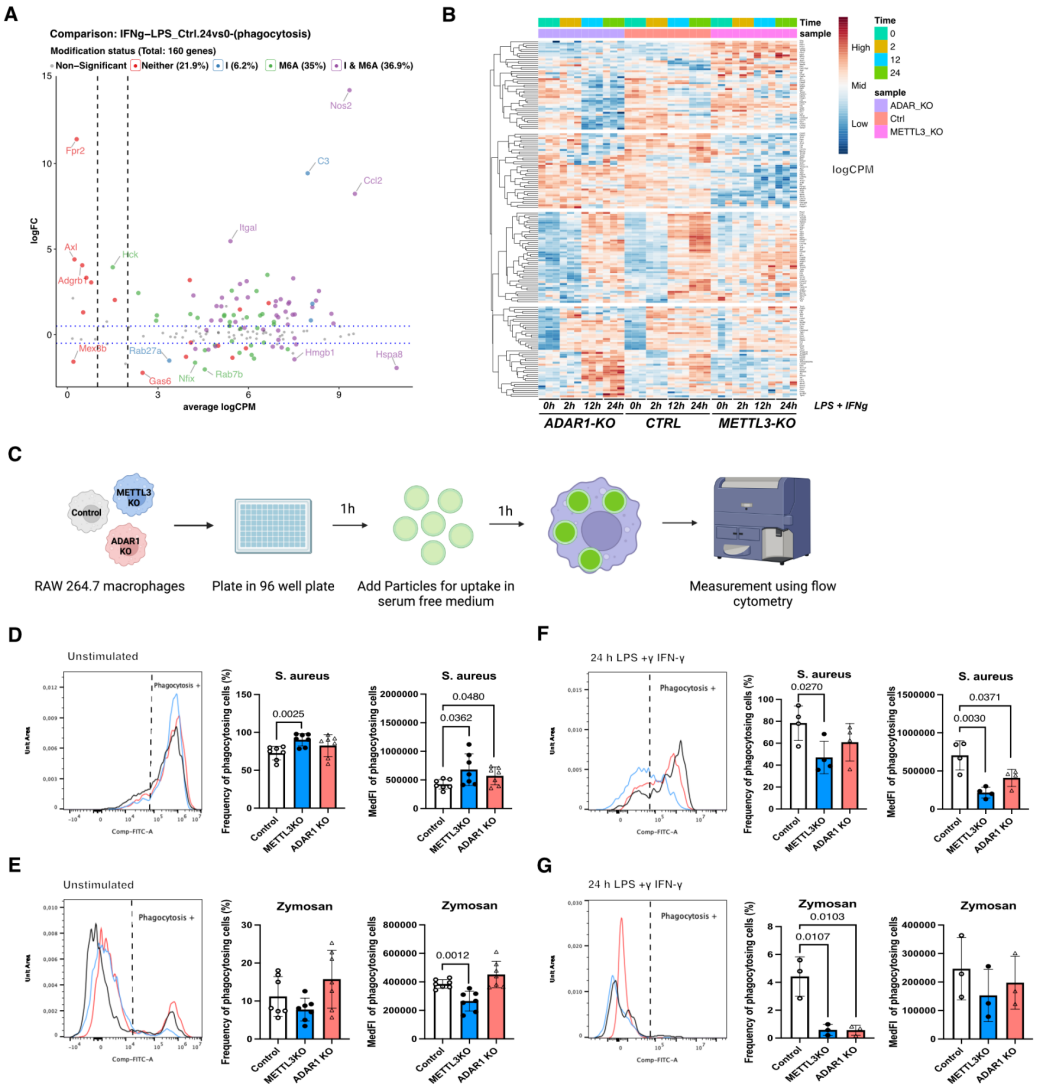

Figure 5. **Impact of Adenosine mRNA modifications on Phagocytosis**. **(A)** MA plot showing mean gene expression (average logCPM) and log fold change (logFC) phagocytosis related genes (GO:0006909) in Control (Ctrl) samples at 24 hours post-LPS-IFNγ treatment, compared with untreated Ctrl samples. Each point represents a gene, with the x-axis indicating mean expression and the y-axis representing differential expression between conditions. Genes are color-coded based on their modification status and differential expression: non-differentially expressed (black), unmodified (red), A-to-I edited (blue), m6A methylated (green), and both edited and methylated (purple). **(B)**Heatmap showing phagocytosis associated gene expression in all conditions. Expression values are presented as logCPM, with rows representing individual genes and columns representing sample groups and replicates (three per sample and condition) at different time points after LPS and IFN-γ treatment. Hierarchical clustering of genes was performed using Euclidean distance of gene expression profiles, and the resulting dendrogram is displayed on the left. **(C)** Schematic representation of phagocytosis assay. **(D-E)** Phagocytosis by non-stimulated Control, METTL3-KO and ADAR1-KO macrophages of *S. aureus* **(D)** and Zymosan **(E)**. **(F-G)** Phagocytosis by Control, METTL3-KO and ADAR1-KO macrophages pre-stimulated for 24h with LPS and IFN-γ of *S. aureus* **(F)** and Zymosan **(G)**. **(D-G)** Unpaired T-test was performed between Ctrl and KOs.

Griesche et al, Figure 6

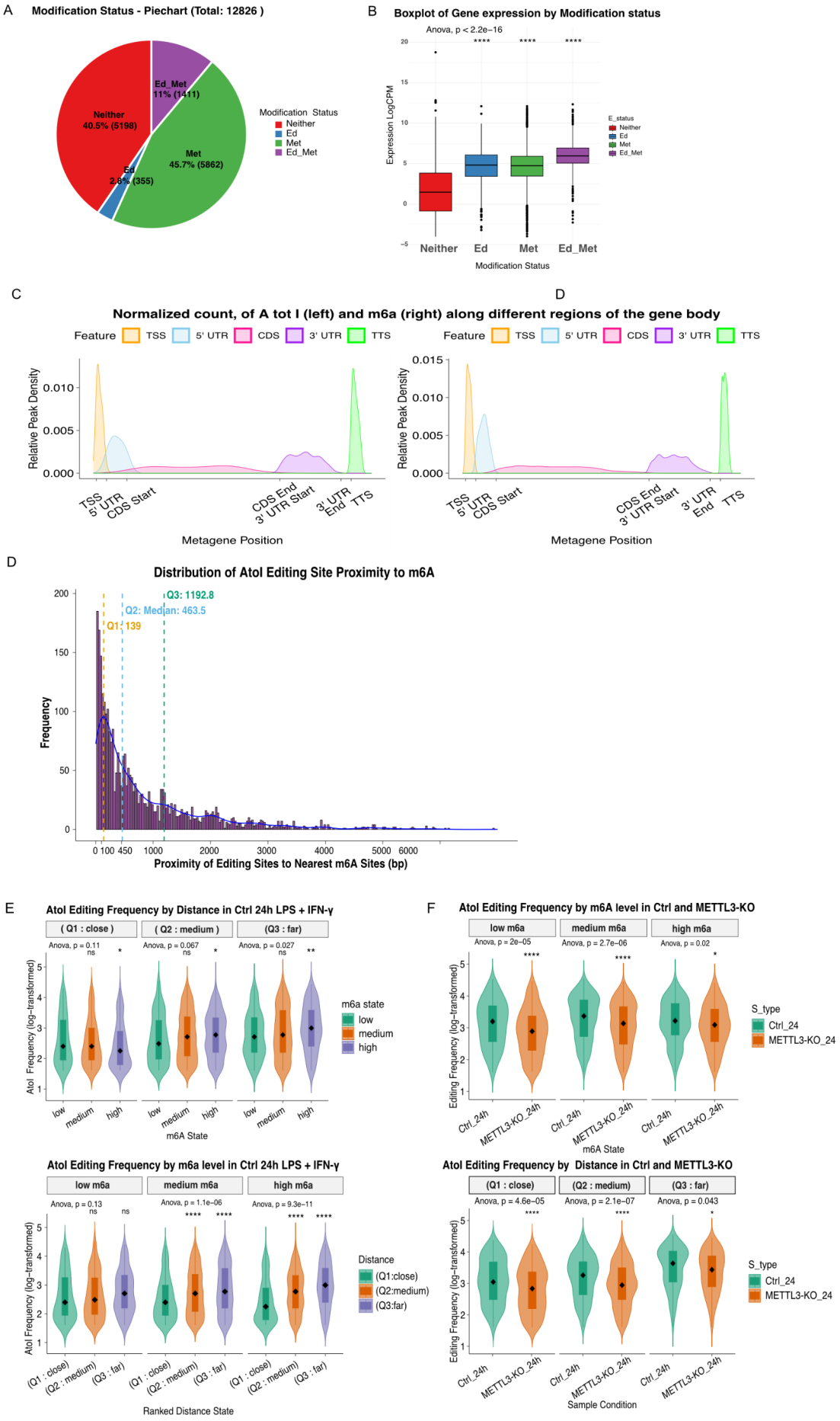

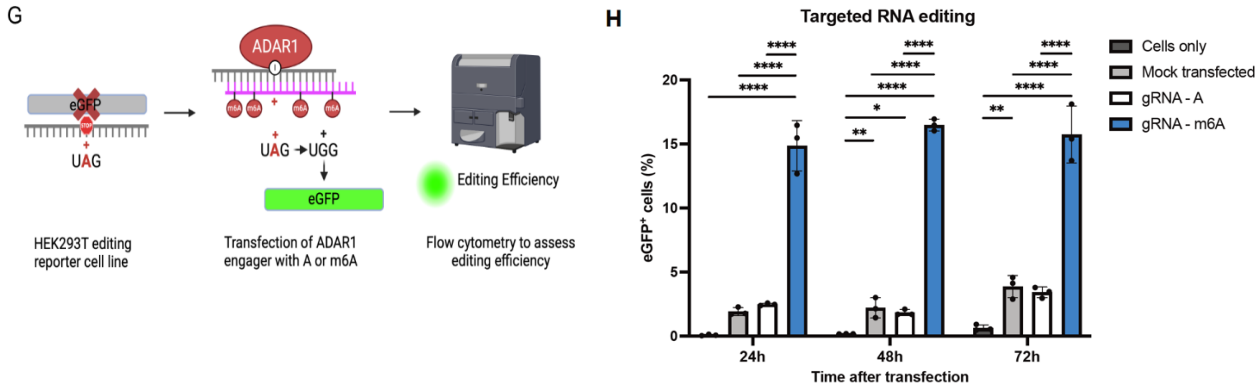

Figure 6: Interdependence between m6A and A-to-I. (**A)** Pie chart illustrating the proportion of all detectable genes in Ctrl samples at 24h post LPS and IFN-γ treatment, classified based on the presence of A-to-I editing, m6A modifications, both, or neither. **(B)** Boxplot displaying global ANOVA and post-hoc t-test results, comparing gene expression levels across different modification groups. **(C)** Normalized distribution of A-to-I and m6A modifications across transcript features. Modification densities were normalized by the relative lengths of each gene region (TSS, 5′ UTR, CDS, 3′ UTR, TTS) to account for feature size differences. Positions were scaled to a metagene coordinate system spanning canonical transcript architecture. **(D)** Genes binned by distance between I and the closer m6A sites in the 3'UTR (≤ 25th quartile, between 25th and 75th quartiles, ≥75th quartile) and grouped based on low, medium and high m6A status of a site. **(E)** A-to-I editing frequency distribution was analyzed across different m6A statuses and A-to-I/m6A distance ranks. Statistical analysis was performed using a one-way ANOVA test, followed by pairwise comparisons using post hoc t-tests. Significance levels are denoted as follows: $*p < 0.05$; $**p < 0.01$; $***p < 0.001$; $****p < 0.0001$. **(F)** The A-to-I site frequency distribution from the previous analysis in (**E**) was compared with the corresponding regions in METTL3-KO, assessing the impact of m6A depletion on editing frequency. **(G)** Schematic representation of GFP reporter assay to assess editing efficiency upon transfection of RNA guide for ADAR1 recruitment. **(H)** Cells were transfected with ADAR1 engaging guide RNA containing normal Adenosine or m6A at all Adenosine sites to induce targeted RNA editing. Editing was analyzed 24h, 48h, and 72h post-transfection based on percentage of GFP-reporter positive cells. One-way ANOVA (multiple comparison) was performed between different conditions ofeach individual time point. Significance levels are denoted as follows: $*p < 0.05$; $**p <0.01$; $***p < 0.001$; $****p < 0.0001$.